

## DATABASE FOR INELASTIC COLLISIONS OF LITHIUM ATOMS WITH ELECTRONS, PROTONS, AND MULTIPLY CHARGED IONS

J. SCHWEINZER,\* R. BRANDENBURG,† I. BRAY,‡ R. HOEKSTRA,§ F. AUMAYR,¶  
R. K. JANEV,|| and HP. WINTER\*\*

\*Max-Planck-Institut für Plasmaphysik, Boltzmannstrasse 2, D-85748 Garching, Germany

†Institut für Allgemeine Physik, TU Wien, Wiedner Hauptstrasse 8-10, A-1040 Vienna, Austria

‡Department of Physics, The Flinders University of South Australia,  
GPO Box 2100, Adelaide 5001, Australia

§KVI Atomic Physics, Zernikelaan 25, 9747 AA Groningen, The Netherlands

¶Institut für Allgemeine Physik, TU Wien, Wiedner Hauptstrasse 8-10, A-1040 Vienna, Austria

||International Atomic Energy Agency, P.O. Box 100, A-1400 Vienna, Austria

\*\*Institut für Allgemeine Physik, TU Wien, Wiedner Hauptstrasse 8-10, A-1040 Vienna, Austria

New experimental and theoretical cross-section data for inelastic collision processes of Li atoms in the ground state and excited states (up to  $n = 4$ ) with electrons, protons, and multiply charged ions have been reported since the database assembled by Wutte et al. [ATOMIC DATA AND NUCLEAR DATA TABLES **65**, 155, 1997] was published. These new data were included in a process of critical data assessment and led to the creation of a new database for the modeling of energetic lithium beams probing fusion edge plasmas. The electron-impact part of the present database covers excitation and ionization, the data having been extended by advanced close-coupling calculations which provide a new standard of quality especially for transitions between excited states. The heavy-particle impact processes include excitation and electron removal (the sum of ionization and electron capture). Hitherto, ion-impact excitation cross sections for lithium (except for the main  $\text{Li}(2s \rightarrow 2p)$  process) were based on scaling relations using the corresponding electron-impact cross sections. We have now performed large-scale atomic orbital close-coupling calculations for a large number of excitation processes as well as new measurements toward development of the new database. The recommended cross sections for the considered processes have been fitted to simple analytic expressions. The analytic-fit expressions and the tables of the parameters entering these analytic fits are here presented. We also present the recommended cross sections in graphical form together with the underlying experimental cross section data if available. © 1999 Academic Press

## CONTENTS

INTRODUCTION .....	240
BASIC DESCRIPTION OF THE APPLIED THEORETICAL METHODS .....	241
Close-Coupling Method for $e^-$ -Li( $nl$ ) Collisions .....	241
Atomic Orbital Close-Coupling for $H^+$ -Li( $nl$ ) Collisions .....	241
PRESENTATION OF DATA .....	242
Collisions with Electrons .....	242
Collisions with Protons .....	244
COMPARISON WITH NEW EXPERIMENTAL DATA FOR PROTON-IMPACT TARGET-EXCITATION PROCESSES .....	245
SCALING RELATIONS FOR COLLISIONS WITH MULTIPLY CHARGED IMPURITY IONS .....	246
EXPLANATION OF TABLES .....	249
TABLES	
I. Fit Parameters for Electron-Impact Target-Excitation Cross Sections of Li( $nl \rightarrow n'l'$ ); $n, n' = 2-4$ ...	250
II. Fit Parameters for Electron-Impact Target-Ionization Cross Sections of Li( $nl$ ); $n = 2, 3$ .....	251
III. Fit Parameters for Proton-Impact Target-Excitation Cross Sections of Li( $nl \rightarrow n'l'$ ); $n = 2, 3; n' = 2-4$ ..	252
IV. Fit Parameters for Proton-Impact Target-Electron-Loss Cross Sections of Li( $nl$ ); $n = 2-4$ .....	253
EXPLANATION OF GRAPHS .....	249
GRAPHS	
I 1-36. Electron-Impact Target-Excitation Cross Sections of Li( $nl \rightarrow n'l'$ ); $n, n' = 2-4$ .....	254
II 1-4. Electron-Impact Target-Ionization Cross Sections of Li( $nl$ ); $n = 2, 3$ .....	263
III 1-29. Proton-Impact Target-Excitation Cross Sections of Li( $nl \rightarrow n'l'$ ); $n = 2, 3; n' = 2-4$ .....	264
IV 1-8. Proton-Impact Target-Electron-Loss Cross Sections of Li( $nl$ ); $n = 2-4$ .....	272

## INTRODUCTION

Cross-section information on inelastic collisions of Li in its ground and excited states with electrons, protons, and multiply charged ions [1] is not only of fundamental interest, but also of considerable practical importance for diagnostics of magnetically confined fusion plasmas by means of Li beam spectroscopy [2-5]. Injection of a

beam of fast (1-10 keV/amu) neutral lithium atoms into the edge of a magnetically confined plasma delivers diagnostic information such as radial electron density profiles, and concentrations and temperatures of impurity ions in a nonperturbing manner. Analysis of the emission lines of injected lithium atoms, which provides informa-

tion on the electron density in the plasma edge, requires knowledge of the populations of all excited atomic states as well as of the Li beam intensity attenuation. Evaluation of the diagnostic raw data relies on modeling the attenuation of the Li( $nl$ ;  $n = 2-4$ ) state beam fractions [2]. The success of this diagnostic method depends strongly on the availability of reliable data for cross sections of inelastic collisions of lithium atoms with plasma particles such as electrons, protons, and multiply charged impurity ions.

Experimental and theoretical cross-section data for collisional processes of Li atoms in the ground state and excited (up to  $n = 4$ ) states with electrons, protons, and multiply charged ions have already been collected in [1, 6]. Cross-section scaling relations based on semiempirical formulae which have to be regarded as rough cross-section estimates for the processes of interest have been used to generate cross sections for processes for which no information was available in the literature. This approach has been extensively used particularly for collisional processes involving excited Li states, and especially for collisions with protons. The expected error for this procedure was in some cases more than 100%.

Recently, detailed investigations of the composition of neutral states [7] along the penetration path of a lithium beam injected into a fusion plasma revealed considerable discrepancies between measurements and the population of specific excited states as derived from beam attenuation models using the atomic collision data of [1]. These differ-

ences triggered experimental and theoretical activities to improve the atomic database.

In this work we use advanced theoretical methods to derive accurate cross sections for all inelastic processes involving collisions with Li atoms, such as single electron capture, ionization, and excitation. These theoretical results are critically tested against the newest available experimental data. In all cases good or at least satisfactory agreement between measurements and theory is found. A similar confidence level of our theoretical results is also expected for cases where no experimental verification is feasible. However, there are still processes where neither calculated nor experimental data exist. The relevant cross sections, which mainly involve Li( $4l$ ) states, are derived by using scaling relations as described in [1]. These are of minor importance from the point of view of fusion plasma diagnostics and thus deserve less attention with respect to accuracy.

The recommended cross sections for the considered processes, generated by (i) critical assessment of available experimental and theoretical data, (ii) by calculations alone, or (iii) by application of scaling relations, have been fitted to analytic expressions which ensure correct asymptotic behavior of the cross sections. These recommended cross sections are presented by giving their analytic-fit expressions and tabulating the values of all parameters entering these analytic fits. We also present the recommended cross sections in graphical form together with the new cross-section data used for their generation.

## BASIC DESCRIPTION OF THE APPLIED THEORETICAL METHODS

### Close-Coupling Method for $e^-$ -Li( $nl$ ) Collisions

In recent years there has been immense progress in the theoretical description of electron-atom scattering. The ever-growing computational resources now allow for very large close-coupling-based calculations where both the discrete and the continuum target spectra are treated to convergence. Here we use the convergent close-coupling (CCC) method, for which the theory has been given by Bray [8]. Briefly, the method uses a set of square-integrable states, obtained by diagonalizing the target Hamiltonian in an orthogonal Laguerre basis, to expand the total wave function of the system. For the lithium target we assume that the frozen-core Hartree-Fock Hamiltonian is a sufficiently accurate representation. Hence, we treat lithium as essentially a one-electron target and electron-lithium scattering as a three-body problem.

The CCC method has already been extensively tested for inelastic electron-lithium scattering. It reproduces the very detailed measurements of  $2p$  excitation

[9], the total ionization cross section and its spin asymmetry [10], and most recently even the differential ionization spin asymmetries [11]. Thus, we have very good reasons to believe in the accuracy of the CCC method in evaluating integrated cross sections for all discrete transitions at all energies. The key issue is obtaining convergence for the transitions of interest with increasing number of expansion states. Generally, the smaller the cross section, the larger the calculation necessary to obtain an accurate result. In practice, we choose a sufficiently large set of states to obtain accurately the most important transitions of interest.

### Atomic Orbital Close-Coupling for $H^+$ -Li( $nl$ ) Collisions

We adopted the semiclassical impact-parameter formalism of the close-coupling (CC) method, assuming straight line trajectories for the projectiles [12, 13]. The time-dependent electronic wave function is expanded in projectile- and target-centered traveling orbitals which

need not necessarily be eigenstates of the corresponding atomic Hamiltonians. Thus, in addition to atomic orbitals (AO), so-called pseudo-states (PS) are also included in our two-center expansion model. While AO represent the bound spectrum of the separated atoms of relevance for the considered inelastic collision process, PS are chosen to account for the formation of transient molecular orbitals as well as to represent the ionization channels. The CC calculation always starts from a linear combination of states which result from diagonalization of the atomic Hamiltonians within the given set of basis states on each center.

The interaction between the core electrons and the “active” electron is described by a model potential. The experimental energy level diagram for Li ( $n \leq 4$ ) is accurately reproduced (with errors  $<0.5\%$ ) by the eigenvalues of the model potential in [14]. One-center couplings between projectile states induced by the electric field of the  $\text{Li}^+$  core are calculated in good approximation by assuming a pure Coulomb interaction potential.

Cross sections for single electron capture (SEC), target excitation (TX), and ionization are derived from AO calculations involving 65 states centered on the proton core and 64 states (AO65\_64) centered on the  $\text{Li}^+$  core. This basis set is used for calculations with initial Li target states  $2s$ ,  $2p$ ,  $3s$ ,  $3p$ , and  $3d$ . On both centers atomic states with principal quantum numbers  $n \leq 4$  are represented in the calculations [13]. All other states are PS, which are orthogonal to the included atomic states of the basis and thus will overlap with higher excited bound states as well as with continuum states ( $l \leq 4$ ). The projection of a pseudo-state on all other, higher excited atomic states with  $n > 4$  gives an estimate of the continuum character of a specific PS. These values are used to calculate approximate cross sections for direct ionization.

Cross sections for target electron loss (TEL, that is, SEC + ionization) are obtained by summing over all cross sections for population of projectile-centered states and the direct ionization cross section of the Li atom.

## PRESENTATION OF DATA

### Collisions with Electrons

The quality and reliability of the database for electron-impact processes are enhanced in comparison to those of the previous database [1] by including the 45-state close coupling (CCC45) cross section data (cf. Close-Coupling Method for  $e^-$ -Li( $nl$ ) Collisions) into the critical data assessment process. The latter consists of cross sections for all possible TX processes  $e^- + \text{Li}(nl) \rightarrow e^- + \text{Li}(n'l')$  with  $n \leq 3$ ,  $n' \leq 4$  and for ionization from levels up to  $3d$ . All calculations are

performed in the impact-energy range from the excitation threshold up to 10 keV. The convergence of the data has been checked by a 64-state calculation (CCC64) at one single impact energy of 200 eV. For all data presented a high level of convergence is reached (cf. Fig. 1). The new data for TX processes have been compared to the recommended cross sections of [1] (cf. Fig. 1). The latter cross sections in the high-energy region had followed the Born cross sections calculated in the Bates–Damgaard approximation for atomic wave functions [16]. For almost all TX processes the CCC45 data also converge toward this

Results from the AO65\_64 calculations are believed to be convergent for impact energies of 1–15 keV. For higher impact energies the TEL cross section is dominated by the ionization process, which is not sufficiently well described with the basis set applied here.

Cross sections for TX were also derived from the AO65\_64 calculations. In addition to the two-center calculations, pure one-center calculations without projectile centered states (AO0\_64) were also performed. These calculations were used to derive TX cross sections at impact energies of 50–500 keV with less computational effort. In this high-impact-energy region the TX process is completely decoupled from electron capture [12], and thus results from AO0\_64 do not differ from those of the much more elaborate calculation AO65\_64. The lowest impact energy  $E_{\min}$ , where one can use the simpler AO0\_64 approach for a specific TX process with excitation energy  $\Delta E$ , is approximately given by  $E_{\min}(\text{keV}) = 7 \cdot \Delta E$ , with  $\Delta E$  in eV. In this way results from both calculations have been used to derive TX cross sections for all  $\text{Li}(nl) \rightarrow \text{Li}(n'l')$  excitations with  $n = 2, 3$ ;  $l = s, p, d$  and  $n' = 2-4$ ;  $l' = s, p, d, f$  in the impact-energy range 1–500 keV. For TX processes with  $\Delta E$  values  $<0.1$  eV the AO0\_64 calculations have been used in the entire impact-energy range.

In general, the coupled equations are solved along straight line trajectories  $R = vt + b$  ( $R$  being the internuclear distance and  $v$  the velocity) from  $vt = -150 a_0$  to  $vt = 150 a_0$  ( $a_0 = \text{Bohr radius}$ ) and for impact parameters  $b$  from 0.3 to  $40 a_0$ . However, for dipole-allowed TX cross sections with small  $\Delta E$  values much larger meshes had to be used. In particular, the AO0\_64 calculations with initial conditions  $3s$ ,  $3p$ , and  $3d$  were done between  $vt = -800 a_0$  and  $vt = 800 a_0$  with impact parameters up to  $150 a_0$ . Even this large impact-parameter range was not sufficient to get convergent results for the  $3p \rightarrow 3d$  TX cross section. For this and other similar cross sections, we suggest scaling the corresponding cross sections for electron impact [1, 15], which should be very accurate in such cases.

performed in the impact-energy range from the excitation threshold up to 10 keV. The convergence of the data has been checked by a 64-state calculation (CCC64) at one single impact energy of 200 eV. For all data presented a high level of convergence is reached (cf. Fig. 1). The new data for TX processes have been compared to the recommended cross sections of [1] (cf. Fig. 1). The latter cross sections in the high-energy region had followed the Born cross sections calculated in the Bates–Damgaard approximation for atomic wave functions [16]. For almost all TX processes the CCC45 data also converge toward this

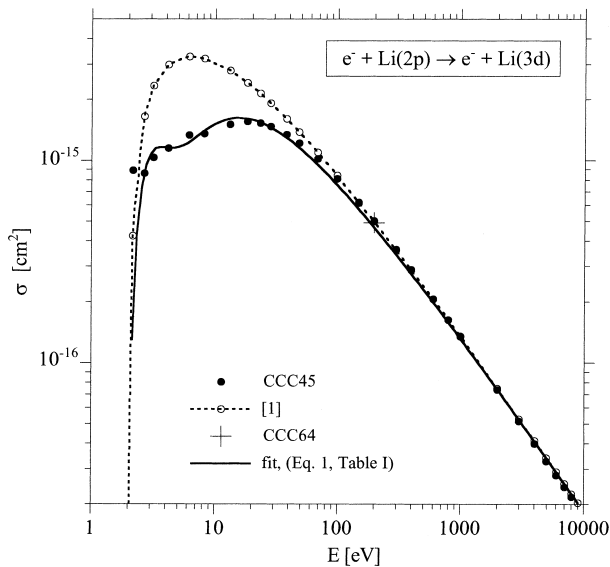


**FIG. 1.** Results from CCC45 and CCC64 calculations for the  $\text{Li}(2p \rightarrow 3d)$  excitation in collisions of  $\text{Li}(2p)$  with electrons in comparison with the corresponding analytic fit (cf. Eq. (1) and Table I) and the recommended cross section of [1].

Born approximation (as represented by [1] in Fig. 1, for example). However, there are exceptions (for example, TX processes which involve the  $4d$  state) where considerable deviations occur, which are believed to be due to small errors in the wave functions of the CCC45 calculations. In such cases we chose the Born cross section in the high-energy region as the recommended one, whereas for low to intermediate energies the original CCC45 results determine the fit.

Experimental data exist for TX processes from the  $\text{Li}(2s)$  ground state. The new CCC45 results agree within 10% of these experimental values in the  $2s \rightarrow 2p$  case. Very good agreement is also found in the  $2s \rightarrow 3s$  case when cascading contributions to the measured  $3s \rightarrow 2p$  emission cross section [17] are taken into account. Larger differences (20–50%) around the cross section maximum are observed for the  $2s \rightarrow 3d$  TX processes, which are most probably due to the polarization and cascade corrections applied by Zajonc and Gallagher [17] to their measured data in order to derive estimations for the TX cross sections. The CCC45 results for all  $\text{Li}(nl \rightarrow n'l')$  transition for  $n = 2, 3$  and  $n' = 2-4$  are shown in Graphs I 1–30 together with the fits from Table I and experimental data where available.

Representation of the cross sections is done by fitting to the following analytic expression with six parameters ( $A_1, \dots, A_6$ ):

$$\sigma_e^{exc}(E/\text{eV})[\text{cm}^2] = \frac{5.984 \times 10^{-16}}{E} \left[ \frac{E - \Delta E}{E} \right]^{A_6} \times \left[ \sum_{j=1}^4 \frac{A_j}{(E/\Delta E)^{j-1}} + A_5 \ln \left( \frac{E}{\Delta E} \right) \right] \quad (1)$$

The fitting functions were chosen to assure asymptotically correct behavior both at low and high impact energies. As a typical example for the quality of the fitting procedure the result of the CCC45 calculation for a single TX process ( $\text{Li}(2p \rightarrow 3d)$ ) is presented in Fig. 1 together with the fit according to Table I. Deviations of the fit from the defining data points are in general below a few percent, except very close to the threshold. Near the latter, however, the error of the underlying data points is also in general larger than at higher impact energies.

In addition to the new results from the CCC45 calculations we also present the fit parameters for the cross section data for  $\text{Li}(4l \rightarrow 4l')$  TX processes in Table I. These cross sections originated from semiempirical formulae [6] and the Born cross sections of [16]. For the  $4l \rightarrow 4f$  processes, however, no data were actually found. Cross sections for these processes have been derived from the fit formula for  $4s \rightarrow 4d$  and  $4p \rightarrow 4d$  for dipole-forbidden and dipole-allowed transitions, respectively, by taking into account the actual statistical weights and excitation energies of the initial and final states involved. These cross sections are plotted in Graphs I 31–36.

Cross sections for ionization of excited  $\text{Li}(nl; n \leq 3)$  are also derived from the CCC45 calculations. Estimates for  $\text{Li}(1s)$  core ionization by applying the Lotz formula [1] indicate only small contributions from  $\text{Li}(1s)$  core ionization to the total ionization cross section and are therefore not added to the results from the CCC45 calculations. The fit formula is given by

$$\sigma_e^{ion}(E/\text{eV})[\text{cm}^2] = \frac{10^{-13}}{EI_{nl}} \left[ A_1 \ln \left( \frac{E}{I_{nl}} \right) + \sum_{j=2}^6 A_j \left( 1 - \frac{I_{nl}}{E} \right)^{j-1} \right], \quad (2)$$

where  $I_{nl}$  is the ionization energy. The CCC45 results and the corresponding fits are shown in Graphs II 1–4; the fit parameters are listed in Table II.

For the ground state  $\text{Li}(2s)$  the recommended curve of [18] agrees well with the result from the CCC45 calculation. The fit formula from [18] together with parameters can be found in [1] and will not be repeated here. Furthermore, ionization from  $\text{Li}(4l)$  states must be estimated by applying the Lotz formula [1, 6] because no other data exist.

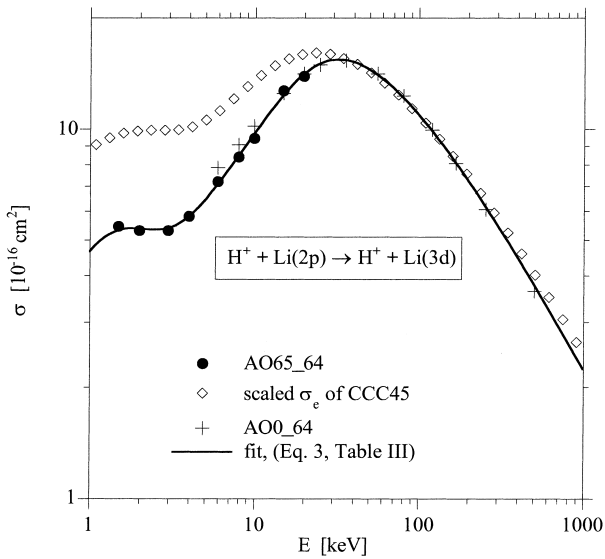


**FIG. 2.** Results from two-center (AO65\_64) and one-center (AO0\_64) close coupling calculations for the  $\text{Li}(2p \rightarrow 3d)$  excitation process in collisions of  $\text{H}^+$  with  $\text{Li}(2p)$  in comparison with the corresponding fit (Eq. (3), Table III) and with the scaled electron impact cross section. The latter has been derived from the CCC45 calculations by applying the scaling relation of [15].

### Collisions with Protons

The scaling of TX cross sections for  $\text{H}^+$  colliding with  $\text{Li}(nl)$  from corresponding cross sections for electrons was always regarded as a weak point of the database of [1]. The mentioned scaling [15] is appropriate in the asymptotic region at high impact energies where Born cross sections for  $\text{H}^+$  and  $e^-$  are the same at the same relative velocity of collision partners, since in this region the mechanism of direct excitation is the same for electrons and protons (cf. Fig. 2). When the impact energy of  $\text{H}^+$  projectiles is lowered, a change from direct excitation to pronounced two-center molecular mechanisms takes place and a general scaling becomes impossible. In the energy range where electron capture is strong or even the dominant inelastic transition, oscillations in the TX cross sections occur in many collision systems involving alkali targets [12, 13, 19]. Furthermore such oscillations are not only restricted to alkali targets, but have been found in other collision systems also [20, 21]. The origin of these oscillations is connected with interference of SEC and TX channels [22]. Attempts to explain these rather unexpected features of TX cross sections in detail can be found in [23–25]. The AO65\_64 calculations were in particular tailored to describe this interaction correctly in order to produce accurate TX cross section in the low-impact-energy range (1–20 keV, cf. Atomic Orbital Close-Coupling For  $\text{H}^+$ – $\text{Li}(nl)$  Collisions).

Because of the structures in the TX cross sections, a fit formula with 12 parameters is necessary to describe the data properly:

$$\sigma_{\text{H}^+}^{\text{TX}}(E/\text{keV})[\text{cm}^2] = 10^{-16} A_1 \left\{ \frac{e^{-A_2/E} (A_{12} + \ln(A_{11} + A_3 E))}{E} + A_4 \frac{e^{-A_5 E}}{E^{A_6}} + A_7 \frac{e^{-A_8/E}}{1 + A_9 E^{A_{10}}} \right\}. \quad (3)$$

The fit parameters for TX processes  $\text{Li}(nl \rightarrow n'l')$  in collisions with  $\text{H}^+$  are listed in Table III. The theoretical data defining the fit for the  $\text{Li}(2p \rightarrow 3d)$  TX cross section are presented in Fig. 2 together with the fitted curve and the scaled electron impact cross section derived from the CCC45 results by using the scaling relation of [15]. As explained earlier, results from two-center (AO65\_64) and pure one-center (AO0\_64) calculations overlap almost perfectly at intermediate and high impact energies. The AO data for  $\text{Li}(nl \rightarrow n'l')$  TX processes with  $n = 2, 3$  and  $n' = 2-4$  are shown in Graphs III 1–29 together with the fits and compared with experimental data where available; the comparison will be further discussed in the next section.

For TX processes between  $\text{Li}(4l)$  states and also for the  $3p \rightarrow 3d$  case the mentioned scaling of  $e^-$  TX cross sections is of course valid, because  $\Delta E[\text{eV}] \ll E[\text{keV}]$ . Dominant contributions to these rather large cross sections take place at impact parameters  $b$  of 40–150  $a_0$ , where no molecular two-center excitation mechanism exists.

The data for TEL processes involving initial  $\text{Li}(nl)$  taken from [1] have been compared with the results from the AO–CC calculation for  $n \leq 3$  in the energy range  $1 < E < 25$  keV, which leads only to minor adjustments of the recommended cross sections. However, for higher  $E$  values where TEL is dominated by ionization, confirmation of the old data from [1, 6] was not possible, because ionization channels were not represented with sufficiently high density of continuum states in the AO65\_64 calculations. Furthermore the AO calculations do not include SEC from the  $\text{Li}(1s)$  core, which is an important contribution to the total TEL cross section in this impact energy range. Therefore, at high impact energy the data from [1, 6] are included without further changes. In addition the data from [6] concerning TEL from  $\text{Li}(4l)$  states are presented. These have been derived by scaling cross sections of lower excited states (cf. [6] for more details).

Two fit functions are presented for TEL from  $\text{Li}(ns; n = 2, 3)$  (nonresonant SEC) and for all other TX processes (almost resonant SEC) by Eqs. (4a) and (4b),

respectively, with the corresponding fit parameters found in Table IV:

$$\sigma_{H^+}^{TEL,Li(ns)}(E/\text{keV})[\text{cm}^2] = 10^{-16} A_1 \left\{ \frac{e^{-A_2/E} \cdot \ln(1 + A_3 E)}{E} + A_4 \frac{e^{-A_5 E}}{E^{A_6} + A_7 E^{A_8}} \right\} \quad (4a)$$

$$\sigma_{H^+}^{TEL,Li(l>0)}(E/\text{keV})[\text{cm}^2] = 10^{-14} A_1 (1 - (e + A_3 E)^{-A_2/E}). \quad (4b)$$

The AO data and fits for  $\text{Li}(nl, n = 2-4)$  are shown in Graphs IV 1-8, where they are also compared with fits from [1].

### COMPARISON WITH NEW EXPERIMENTAL DATA FOR PROTON-IMPACT TARGET-EXCITATION PROCESSES

In this section we will compare TX cross sections of the new database, which were generated as described from theoretical results only, with new experimental data measured at the IAP Vienna [7] and at the KVI Groningen [26] by means of photon spectroscopy. TX cross sections have to be transformed into the respective emission cross sections for comparison with experimental data. In Eqs. (5)–(8) we give the relation between theoretical emission (cascading contributions are taken into account up to  $\text{Li}(4f)$ ) and TX cross sections, which will be used in Figs. 3, 4, 5, and 6 for comparison with the measured cross sections for  $3d \rightarrow 2p$ ,  $3p \rightarrow 2s$ ,  $4s \rightarrow 2p$ , and  $4d \rightarrow 2p$  emission, respectively, in collisions of  $\text{Li}(2s)$  with protons:

$$\sigma(3d \rightarrow 2p) = \sigma(3d) + 0.2\sigma(4p) + \sigma(4f) \quad (5)$$

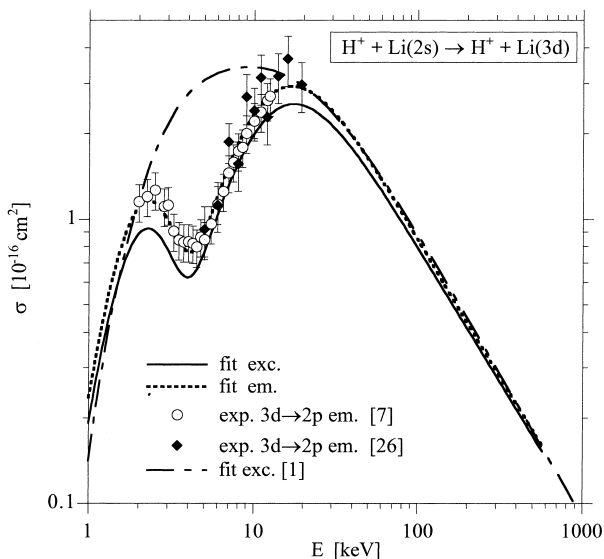


**FIG. 3.** TX and emission cross sections from the new and old database in comparison with measurements for the  $3d \rightarrow 2p$  emission cross sections from two measurements.

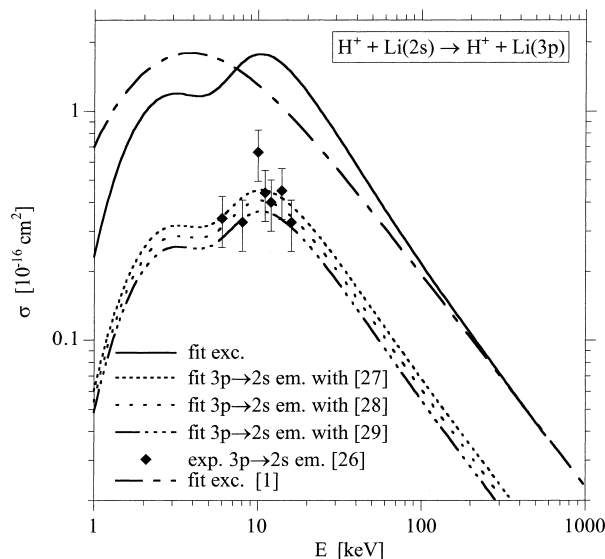


**FIG. 4.** TX and emission cross sections from the new and old database in comparison with experimental data for the  $3p \rightarrow 2s$  emission process in collisions of protons with  $\text{Li}(2s)$ . Theoretical emission cross sections shown are derived using transition probabilities from three different sources (cf. text).

$$\sigma(3p \rightarrow 2s) = 0.237\sigma(3p) + 0.1\sigma(4s) + 0.055\sigma(4d) \quad (6)$$

$$\sigma(4s \rightarrow 2p) = 0.575\sigma(4s) + 0.16\sigma(4p) \quad (7)$$

$$\sigma(4d \rightarrow 2p) = 0.77\sigma(4d). \quad (8)$$

Transition probabilities for the branching ratios are taken from [27].

The  $3d \rightarrow 2p$  emission (“fit em.” in Fig. 3) and  $2s \rightarrow 3d$  TX (“fit exc.” in Fig. 3) cross sections differ only by cascade contributions from higher excited states, because only one strong transition from  $3d$  is allowed by selection rules. As seen in Fig. 3, excellent agreement between the two independent measurements and the emission cross sec-

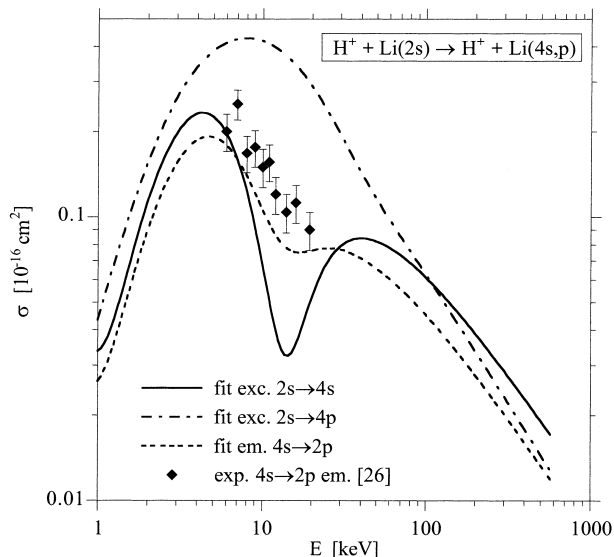


**FIG. 5.** TX and emission cross sections from the new database in comparison with experimental data for the  $4s \rightarrow 2p$  emission process in collisions of protons with Li(2s).

tion curve derived from the new database is found. For further comparison the recommended curve from [1] is also shown. As expected, old (based on the scaled electron cross sections) and new data join each other in the asymptotic region of high energy. However, in the energy region between 3 and 10 keV—the region most important for plasma diagnostic purposes—the two curves deviate from each other by up to a factor of 3.

In Fig. 4, a similar comparison is presented for the  $3p \rightarrow 2s$  emission cross section. The transition probability for Li( $3p \rightarrow 2s$ ) is found in the literature [27–29] with values differing by 30%, whereas for all other transitions of Li I much less uncertainty is found. Emission cross sections derived from TX therefore depend on the chosen reference used for calculating branching ratios. The agreement between theoretical and experimental results is excellent.

## SCALING RELATIONS FOR COLLISIONS WITH MULTIPLY CHARGED IMPURITY IONS

The behavior of TX cross sections with respect to a scaling relation with projectile charge state  $q$  and mass  $m$  (in amu), derived from a three-state close-coupling dipole approximation [30] and represented in the following equation, has been analyzed in [12]:

$$\sigma^{red} = \frac{\sigma}{q}; \quad E^{red} = \frac{E}{qm}. \quad (9)$$

In the case of the main TX process Li( $2s \rightarrow 2p$ ) this well-established scaling is appropriate for higher impact

energies  $E^{red} \geq 6$  keV/amu only [13]. For lower energies no regular behavior has been found.

Although the measured  $4s \rightarrow 2p$  emission cross sections are not dominated by a single TX process (cf. Eq. (7)), but is rather a combination of two TX cross sections with rather different behavior with impact energy (cf. Fig. 5), satisfactory agreement between theoretical and measured emission cross sections is found. Underestimation of experimental values is most probably due to the omission of higher cascade contributions in the theoretical emission cross section. (cf. Eq. (7)).

For the  $4d \rightarrow 2p$  emission cross section no cascading contribution from higher excited states could be provided by the AO-CC results (cf. Basic Description of the Applied Theoretical Methods), which leads to a small underestimation of the experimental cross sections as seen in Fig. 6.

Altogether, we have verified by comparison with experimental data our theoretical approach, which is the basis for the new database.

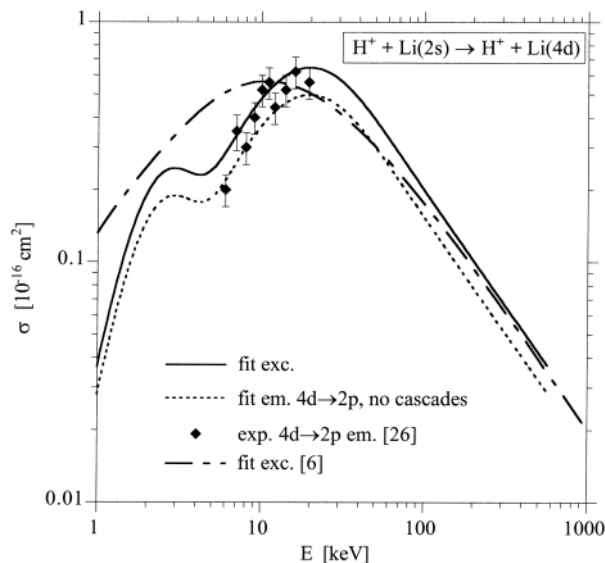


**FIG. 6.** TX and emission cross sections from the new and old database in comparison with experimental data for the  $4d \rightarrow 2p$  emission process in collisions of protons with Li(2s).

In Fig. 7 we present experimental data for Li( $3d \rightarrow 2p$ ) emission cross sections for collisions of Li(2s) with different projectiles ( $H^+$ ,  $He^{2+}$ ,  $N^{9+}$ ). These experimental data are compared to the recommended curve of the  $H^+ + Li(2s) \rightarrow H^+ + Li(3d)$  TX cross section (no cascade contributions are taken into account), which should serve as a general curve in the case of perfectly valid scaling relation. One observes that there is no overlap between the data for multiply charged ions and the data for proton impact for

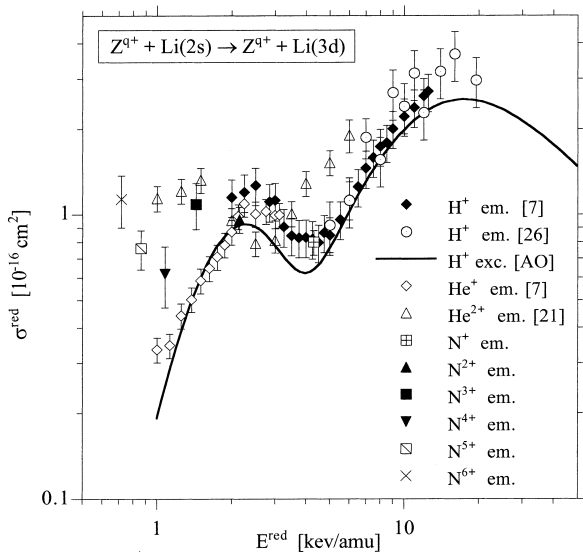


**FIG. 7.** Scaled experimental  $\text{Li}(3d \rightarrow 2p)$  emission cross sections in collisions of  $\text{Li}(2s)$  with  $\text{H}^+$ ,  $\text{He}^{q+}$ , and  $\text{N}^{q+}$  ( $q = 1-6$ ), which are compared with the new  $\text{Li}(2s \rightarrow 3d)$  TX cross section for proton impact.

energies  $E^{\text{red}} > 6$  keV/amu. Therefore the validity of the scaling relations is not experimentally demonstrated in the high-impact-energy range (as will be further discussed in [26]), but, however, can be assumed with high probability for  $E^{\text{red}} > 8$  keV/amu.

With decreasing impact energy we observe more and more scatter within the data points corresponding to different  $q$  values as well as increasing deviation of the experimental data of the heavier ions from the expected general TX cross-section curve. This situation is rather unsatisfactory from the point of view of the Li beam diagnostic application, where the above scaling (Eq. (9)) is used generally. However, in most cases concentrations of multiply charged impurity ions in modern fusion plasmas are rather low, which reduces the accuracy demands on such cross sections. Application of the diagnostic approach to helium discharges, however, should preferably use accurate cross-section data instead of relying on scaling from the atomic database for protons, at least for the dominant TX processes.

The scaling of TEL cross sections for impact of multiply charged ions on  $\text{Li}(nl; n = 2, 3)$  has already been presented in [1] and will not be repeated here.

## References

1. D. Wutte, R. K. Janev, F. Aumayr, M. Schneider, J. Schweinzer, J. J. Smith, and HP. Winter, *ATOMIC DATA AND NUCLEAR DATA TABLES* **65**, 155 (1997)

2. J. Schweinzer, E. Wolfrum, F. Aumayr, M. Pöckl, HP. Winter, R. P. Schorn, E. Hintz, and A. Unterreiter, *Plasma Phys. Controlled Fusion* **34**, 1173 (1992)
3. R. P. Schorn, E. Wolfrum, F. Aumayr, E. Hintz, D. Rusbüldt, and HP. Winter, *Nucl. Fusion* **32**, 351 (1992)
4. E. Wolfrum, F. Aumayr, D. Wutte, HP. Winter, E. Hintz, D. Rusbüldt, and R. P. Schorn, *Rev. Sci. Instrum.* **64**, 2285 (1993)
5. J. Schweinzer, F. Aumayr, P. Platzer, M. Schneider, D. Wutte, and HP. Winter, *Comput. Phys. Commun.* **88**, 83 (1995)
6. R. Janev, J. J. Smith, F. Aumayr, D. Wutte, M. Schneider, HP. Winter, and J. Schweinzer, IAEA Report INDC(NDS)-267 (1993)
7. R. Brandenburg, J. Schweinzer, S. Fiedler, F. Aumayr, and HP. Winter, *Plasma Phys. Controlled Fusion* **41**, 471 (1999)
8. I. Bray, *Phys. Rev. A* **49**, 1066 (1994)
9. V. Karaganov, I. Bray, and P. J. O. Teubner, *J. Phys. B* **31**, L187 (1998)
10. I. Bray, *J. Phys. B* **28**, L247 (1995)
11. M. Streun, G. Baum, W. Blask, J. Rasch, I. Bray, D. V. Fursa, S. Jones, D. H. Madison, H. R. J. Walters, and C. T. Whelan, *J. Phys. B* **31**, 4401 (1998)
12. J. Schweinzer, D. Wutte, and HP. Winter, *J. Phys. B* **27**, 137 (1994)
13. R. Brandenburg, J. Schweinzer, F. Aumayr, and HP. Winter, *J. Phys. B* **31**, 2585 (1998)
14. G. Peach, H. E. Saraph, and M. J. Seaton, *J. Phys. B* **21**, 3669 (1988)
15. D. R. Bates and G. Griffing, *Proc. Phys. Soc.* **63**, 961 (1953)
16. I. I. Sobelman, L. A. Vainshtein, and E. A. Yukov, *Excitation of Atoms and Broadening of Spectral Lines* (Springer-Verlag, Berlin, 1981)
17. A. Zajonc and A. Gallagher, *Phys. Rev. A* **20**, 1393 (1979)
18. M. A. Lennon, K. L. Bell, H. B. Gilbody, J. G. Hughes, A. E. Kingston, M. J. Murray, and F. J. Smith, *J. Phys. Chem. Ref. Data* **17**, 1285 (1988)
19. G. Horvath, J. Schweinzer, HP. Winter, and F. Aumayr, *Phys. Rev. A* **54**, 3022 (1996)
20. R. E. Olson, J. Pascale, and R. Hoekstra, *J. Phys. B* **25**, 4241 (1992)

21. M. P. Hughes et al., *J. Phys. B* **27**, 1143 (1994)
22. W. Fritsch et al., *Phys. Rev. A* **44**, 5686 (1991)
23. D. R. Schultz and P. S. Krstic, *Phys. Rev. Lett.* **78**, 2720 (1997)
24. D. S. Krstic, C. O. Reinhold, and D. R. Schultz, *J. Phys. B* **31**, L155 (1998)
25. J. P. Hansen, L. Kocbach, S. A. Synnes, J. B. Wang, and A. Dubois, *Phys. Rev. A* **57**, R4086 (1998)
26. J. W. Turkstra, D. Meyer, R. Hoekstra, R. Morgenstern, and J. Schweinzer, submitted for publication
27. W. L. Wiese, M. W. Smith, and B. M. Glennon, *Atomic Transition Probabilities (NSRDS-NBS4)*, Vol. 1 (U.S. Government Printing Office, Washington, DC, 1966)
28. A. Lindgard and S. E. Nielsen, *ATOMIC DATA AND NUCLEAR DATA TABLES* **19**, 533 (1977)
29. D. A. Verner, E. M. Verner, and G. F. Ferland, *ATOMIC DATA AND NUCLEAR DATA TABLES* **64**, 1 (1996)
30. R. K. Janev and L. P. Presnyakov, *J. Phys. B* **13**, 4233 (1980)
31. D. Leep and A. Gallagher, *Phys. Rev. A* **10**, 1082 (1974)
32. L. Vuskovic, S. Trajmar, and D. F. Register, *J. Phys. B* **15**, 2517 (1982)
33. I. P. Zapesochnyi, I. V. Postoi, and I. S. Aleksakhin, *Sov. Phys. JETP* **41**, 865 (1975)
34. F. Aumayr, M. Fehringner, and HP. Winter, *J. Phys. B* **17**, 4185 (1984)

## EXPLANATION OF TABLES

**TABLE I. Fit Parameters for Electron-Impact Target-Excitation Cross Sections of  $\text{Li}(nl \rightarrow n'l')$ ;  $n, n' = 2-4$**

$nl-n'l'$	Initial-final states of the Li atom
$\Delta E$	Excitation energy of the TX process, in eV
$A_1, \dots, A_6$	Fit parameters $A_1, \dots, A_6$ in Eq. (1)
source	Source providing data for deriving the fit parameters

**TABLE II. Fit Parameters for Electron-Impact Target-Ionization Cross Sections of  $\text{Li}(nl)$ ;  $n = 2, 3$**

$nl$	Initial state of the Li atom
$I_{nl}$	Ionization energy in eV
$A_1, \dots, A_6$	Fit parameters $A_1, \dots, A_6$ in Eq. (2), derived from CCC45 calculations

**TABLE III. Fit Parameters for Proton-Impact Target-Excitation Cross Sections of  $\text{Li}(nl \rightarrow n'l')$ ;  $n = 2, 3$ ;  $n' = 2-4$**

$nl-n'l'$	Initial-final states of the Li atom
$A_1, \dots, A_{12}$	Fit parameters $A_1, \dots, A_{12}$ in Eq. (3) derived from AO calculations; for TX cross sections between $\text{Li}(4l)$ states and the $3p \rightarrow 3d$ transition, see text and [1]

**TABLE IV. Fit Parameters for Proton-Impact Target-Electron-Loss Cross Sections in  $\text{Li}(nl)$ ;  $n = 2-4$**

$nl$	Initial state of the Li atom
$A_1, \dots, A_8$	Fit parameters $A_1, \dots, A_8$ in Eqs. (4a) and (4b) derived from the AO65_64 calculations and from [1]

## EXPLANATION OF GRAPHS

**GRAPHS I 1-36. Electron-Impact Target Excitation Cross Sections of  $\text{Li}(nl \rightarrow n'l')$ ;  $n, n' = 2-4$**

Plotted are the fitted cross sections from Eq. (1), the CCC45 calculated data (Graphs I 1-30) from which fit parameters are derived, and experimental data where available.

**GRAPHS II 1-4. Electron-Impact Target-Ionization Cross Sections of  $\text{Li}(nl)$ ;  $n = 2, 3$**

Plotted are the fitted cross sections from Eq. (2) and the CCC45 calculated data from which the fit parameters are derived.

**GRAPHS III 1-29. Proton-Impact Target-Excitation Cross Sections of  $\text{Li}(nl \rightarrow n'l')$ ;  $n = 2, 3$ ;  $n' = 2-4$**

Plotted are the fitted cross sections from Eq. (3), the AO calculated data from which fit parameters are derived, experimental photon emission data where available, and fits to the emission data derived from the TX cross sections.

**GRAPHS IV 1-8. Proton-Impact Target-Electron-Loss Cross Sections of  $\text{Li}(nl)$ ;  $n = 2-4$**

Plotted are the fitted cross sections from Eqs. (4a) and (4b) and the AO65\_64 calculated data from which fit parameters are derived, and the fitted data from [1].

TABLE I. Fit Parameters for Electron-Impact Target-Excitation Cross Sections  
of  $\text{Li}(nl \rightarrow n'l')$ ;  $n, n' = 2-4$   
See page 249 for Explanation of Tables

$nl-n'l'$	$\Delta E$	A 1	A 2	A 3	A 4	A 5	A 6	source
2s-2p	1.847	-29.466	10.106	128.32	-86.415	58.696	0.77758	CCC45
2s-3s	3.372	4.50	-11.393	9.2699	1.8822	0	0.32060	CCC45
2s-3p	3.833	2.2138	-4.3282	4.4758	0	0	0.25068	CCC45
2s-3d	3.877	8.20	-8.2458	-6.4716	12.953	0	0.61774	CCC45
2s-4s	4.34	0.92600	-1.1803	-1.2032	2.0279	0	0.053105	CCC45
2s-4p	4.52	0.054550	1.0983	-1.00	0.12220	0.150	0.12917	CCC45
2s-4d	4.539	1.8676	-1.8193	0.26790	0	0	0.25478	CCC45
2s-4f	4.54	0.250	3.3341	-6.5182	4.9176	0	0.90017	CCC45
2p-3s	1.525	-12.287	7.9788	21.593	-10.454	10.136	0.35903	CCC45
2p-3p	1.986	10.353	-22.590	21.347	0	0	0.33146	CCC45
2p-3d	2.03	-20.091	-78.831	306.52	-146.03	38.767	+1.7130	CCC45
2p-4s	2.493	-0.45472	6.2003	-23.437	25.556	0.70915	1.1250	CCC45
2p-4p	2.673	2.4654	-3.9177	4.7847	0	0	0.78931	CCC45
2p-4d	2.692	4.8531	-40.566	83.492	-46.007	4.5560	0.57257	CCC45
2p-4f	2.693	2.1425	24.042	-77.016	62.941	0.24507	0.79098	CCC45
3s-3p	0.461	-678.58	805.29	0	0	439.50	0.78903	CCC45
3s-3d	0.505	96.957	-309.15	1089.2	0	0	2.4374	CCC45
3s-4s	0.968	18.409	-72.121	34.575	109.59	0.94483	1.2021	CCC45
3s-4p	1.148	8.4345	-10.284	0	25.887	1.9035	0.62176	CCC45
3s-4d	1.167	10.233	407.74	-2173.8	3286.7	0	3.7253	CCC45
3s-4f	1.168	28.327	100.47	-421.76	419.50	0	1.00	CCC45
3p-3d	0.044	186.96	-1032.5	2307.1	0	230.05	2.6800	CCC45
3p-4s	0.507	-117.31	196.06	-78.658	0	64.033	0.062851	CCC45
3p-4p	0.687	49.0	-218.58	392.42	-201.84	0	0.61809	CCC45
3p-4d	0.706	-202.18	335.80	-132.60	0	113.64	0.28384	CCC45
3p-4f	0.707	115.93	-99.313	-319.37	758.96	0	2.3647	CCC45
3d-4s	0.463	5.80	-13.713	54.729	-44.469	0	0.69859	CCC45
3d-4p	0.643	2.2291	-10.245	42.434	-28.528	2.2158	0.21465	CCC45
3d-4d	0.662	43.0	-142.81	226.64	-110.26	0	0.69480	CCC45
3d-4f	0.663	-221.53	-371.82	3313.2	-1906.1	221.29	3.7250	CCC45
4s-4p	0.18	0.072489	816.84	0	0	992.70	1.1539	[6]
4s-4d	0.199	384.65	-489.77	382.85	0	0	0.51756	[6]
4s-4f	0.2	492.35	-626.91	490.05	0	0	0.51756	[6]
4p-4d	0.019	0.11050	126.57	382.62	0	778.86	0.92249	[6]
4p-4f	0.02	538.51	-685.678	535.99	0	0	0.51756	[6]
4d-4f	0.001	0.1547	177.198	535.668	0	1090.4	0.92249	[6]

TABLE II. Fit Parameters for Electron-Impact Target-Ionization Cross Sections  
of  $\text{Li}(nl)$ ;  $n = 2, 3$

See page 249 for Explanation of Tables

$n l$	$I_{nl}$	A 1	A 2	A 3	A 4	A 5	A 6
$2p$	3.5430	0.075347	0.18820	-0.28343	1.5382	-1.8550	1.3411
$3s$	2.0180	5.55e-15	0.34812	-0.29262	0.34264	0.99613	-0.82395
$3p$	1.5570	0.11218	0.24966	-1.0074	1.8549	-1.1973	0.48164
$3d$	1.5130	0.023390	0.37229	0.011639	-3.1118	7.7385	-4.5292

TABLE III. Fit Parameters for Proton-Impact Target-Excitation Cross Sections of  $\text{Li}(nl \rightarrow n'l')$ ;  $n = 2, 3$ ;  $n' = 2-4$   
See page 249 for Explanation of Tables

$nl-n'l'$	A1	A2	A3	A4	A5	A6	A7	A8	A9	A10	A11	A12
2s-2p	890.49	1.6973	0.069996	0.00066567	0.044648	-1.0953	0	0	0	0	1	0
2s-3s	5.863	4.2883	6.8323	0.26832	0.67713	-1.8562	-0.40274	1.1356	0.0005	2.7408	1	0
2s-3p	0.65745	4.3251	6.0806e+11	-0.022124	1.1023	-5.7063	56.764	24.563	0.0093162	2.64	1	0
2s-3d	3.4985	15.139	1.6614e+08	0.99391	2.8969	-6.3543	12.577	39.279	0.0064179	2.37	1	0
2s-4s	1.4655	16.32	1.7825	0.43818	0.42587	-1.3667	-0.80309	1.0762	0.04	1.9618	1	0
2s-4p	0.54998	7.9996	547.8	0.04693	0.14368	-1.3119	0.74066	2.879	0.15388	1.27	1	0
2s-4d	0.078979	37.545	1	4.1593	2.2075	-5.4485	13.281	8.0469	0.0005	2.2842	0	272.81
2s-4f	0.23326	18.753	1	1.7568	2.4424	-5.9291	-7.0469	10.042	0.025	1.0508	0	202.41
2p-3s	104.22	10.269	0.20822	0.041493	0.66082	-1.5575	-0.0011208	-2.4703	1.3388e-05	1.59	1	0
2p-3p	16.639	1.091	1	5.5038	2.5522	-2.5638	1.5021	12.193	0.025	1.5991	0	-0.75556
2p-3d	447.72	7.5823	0.15353	0.015268	0.31379	-1.1443	-0.10783	4.8259	0.02	1.7569	1	0
2p-4s	7.7901	4.4552	0.089696	0.018676	0.038835	1.5048	0.055521	136.78	0.0027993	1.8	1	0
2p-4p	0.43521	4.3948	608.91	256.4	0.63753	0.31571	-84.829	-0.65447	0.15006	1	0	608.91
2p-4d	-1.7894	2.7041	1.9	-0.1842	0.45099	-1.5348	-2.5092	10.389	0.01	1.0524	0	-2.5386
2p-4f	7.4324	13.618	1	0.18168	0.40864	-1.054	-0.1499	1.295	0.01	1.0361	0	9.3708
3s-3p	0.31203	-6.2025	1	50.837	0.38838	-2.1872	2349.6	3.8901	0.040084	0.95	0	0.68525
3s-3d	4.4094	2.0987	1	33.917	0.49168	-1.1262	0	0	0	0	0	246.16
3s-4s	0.54407	27.847	1	-254.05	1.2034	-0.63629	-9983.2	1.9131	-15	2.6501	0	539.78
3s-4p	21.499	2.5093	1	-0.91164	2.469	-6.4657	3.0077	-2.1779	54.734	0.85	0	4.2732
3s-4d	3.6606	14.845	1	7.3581	1.0571	-1.9454	47.54	68.16	-0.65	1.0493	0	75.372
3s-4f	28.185	0.76087	1	0.031421	1.3193	-5.9428	-290.91	15.641	-0.83447	2	0	1.0769
3p-4s	694.87	-0.060939	0.17257	-0.16419	0.066701	0.20013	0	0	0	0	1	0
3p-4p	5.6726	0.67142	1	-62.696	0.28219	0.21339	0	0	0	0	0	93.455
3p-4d	635.13	40.448	16.458	0.027783	0.14875	-0.982	0	0	0	0	1	0
3p-4f	150.06	3.317	3.2153	0.079889	0.02093	-0.14656	0	0	0	0	1	0
3d-4s	4.7923	0.46114	1437.4	-5.2521	0.54921	0.55062	0	0	0	0	1	0
3d-4p	18.128	0.13577	1	0.018608	1.1043	-5.4651	-4.6651	0.14713	0.78327	1.5	0	3.2626
3d-4d	28.857	9.2188	1	0.0080717	1.5786	-7.1542	1.3987	1.0674	0.032486	1.5	0	8.3812
3d-4f	8.9744	15.822	1	-0.037089	0.16502	-2.5493	5.6009	1.0531	0.0044742	1	0	524.38

TABLE IV. Fit Parameters for Proton-Impact Target-Electron-Loss Cross Sections  
of  $\text{Li}(nl)$ ;  $n = 2-4$

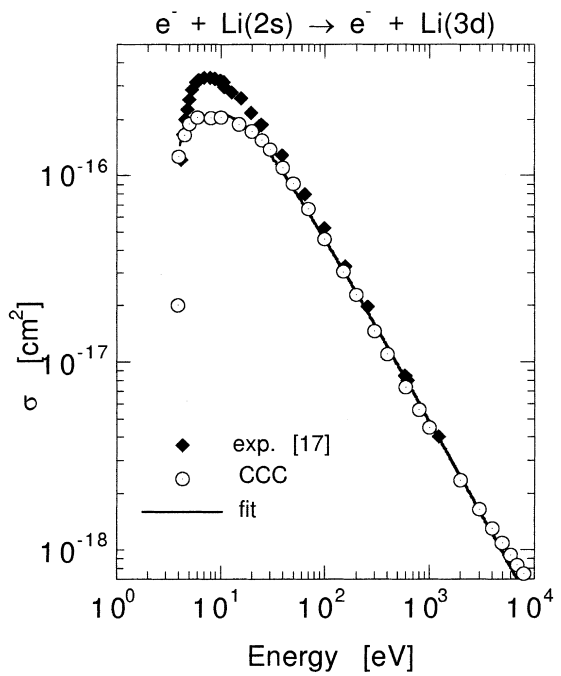
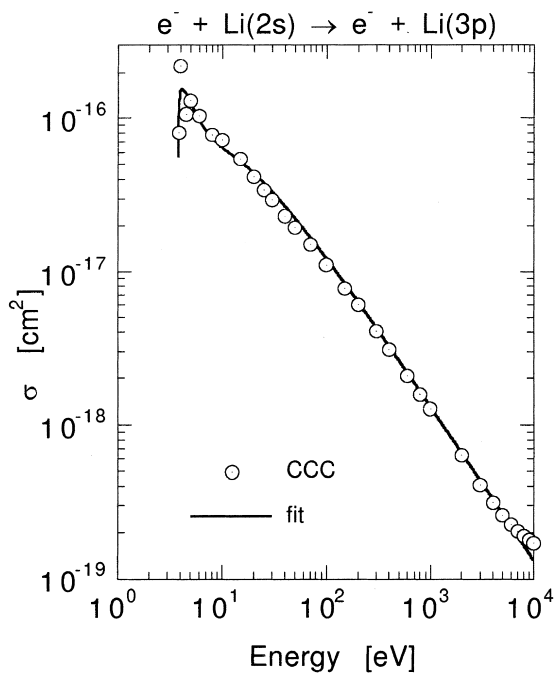
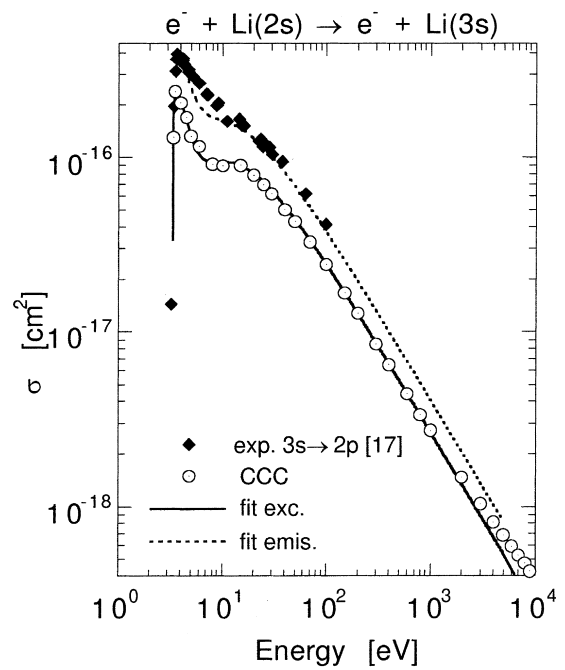
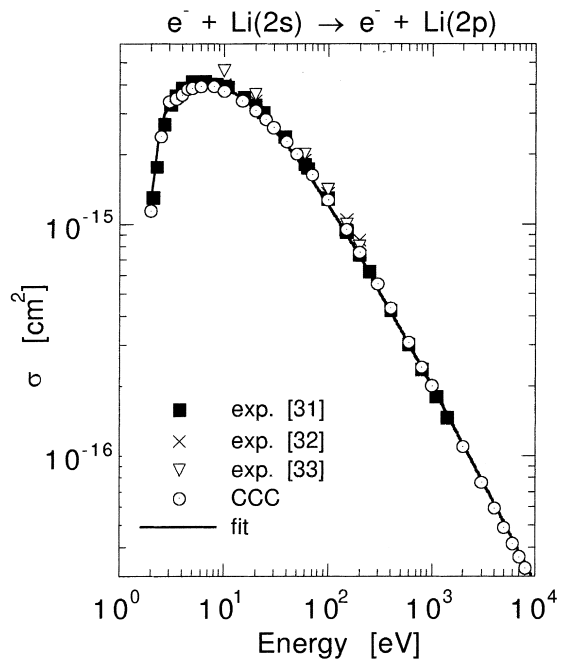
See page 249 for Explanation of Tables

$n l$	A 1	A 2	A 3	A 4	A 5	A 6	A 7	A 8
$2s$	29.172	9.5281	4097.6	11.105	0.13404	0.61553	16.25	-1.588
$2p$	0.94189	5.6482	0.001491	0	0	0	0	0
$3s$	70.99	1.9579	86264.0	8.4351	0.56675	-0.10664	0	0
$3p$	3.3687	3.9346	0.0017891	0	0	0	0	0
$3d$	3.1948	4.6444	0.0012749	0	0	0	0	0
$4s$	16.24	1.1957	0.0016519	0	0	0	0	0
$4p$	11.041	2.0596	0.0017696	0	0	0	0	0
$4d$	10.191	2.62	0.0010166	0	0	0	0	0
$4f$	9.98	2.62	0.0010166	0	0	0	0	0

GRAPHS I 1-36. Electron-Impact Target-Excitation Cross Sections

of  $\text{Li}(nl \rightarrow n'l')$ ;  $n, n' = 2-4$

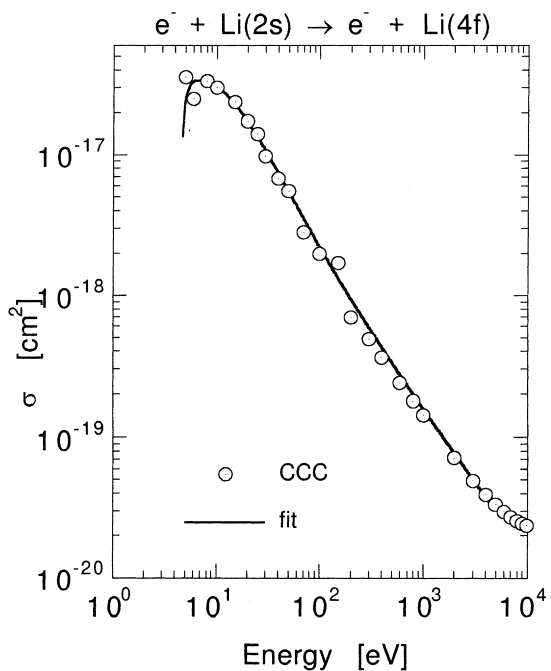
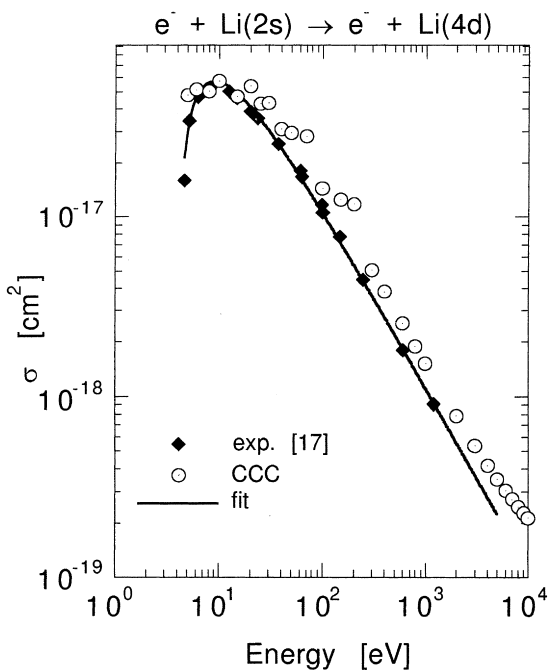
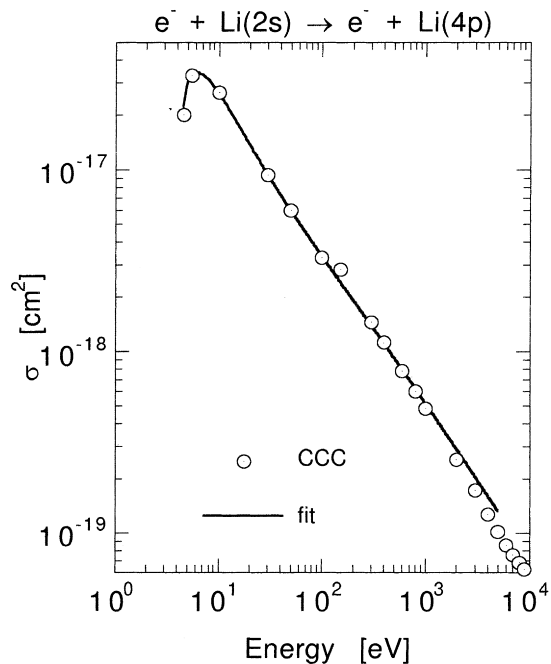
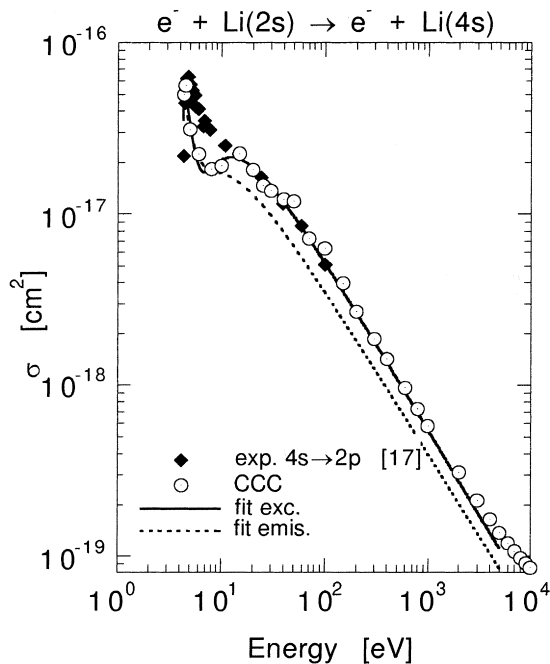
See page 249 for Explanation of Graphs



GRAPHS I 1-36. Electron-Impact Target-Excitation Cross Sections

of  $\text{Li}(nl \rightarrow n'l')$ ;  $n, n' = 2-4$

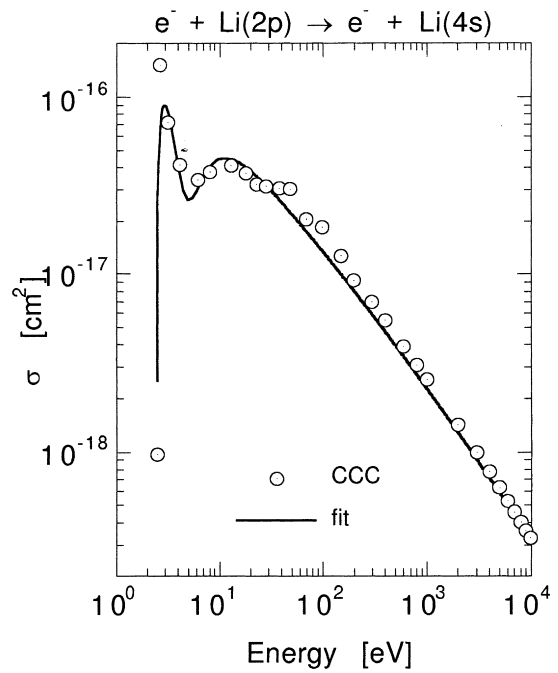
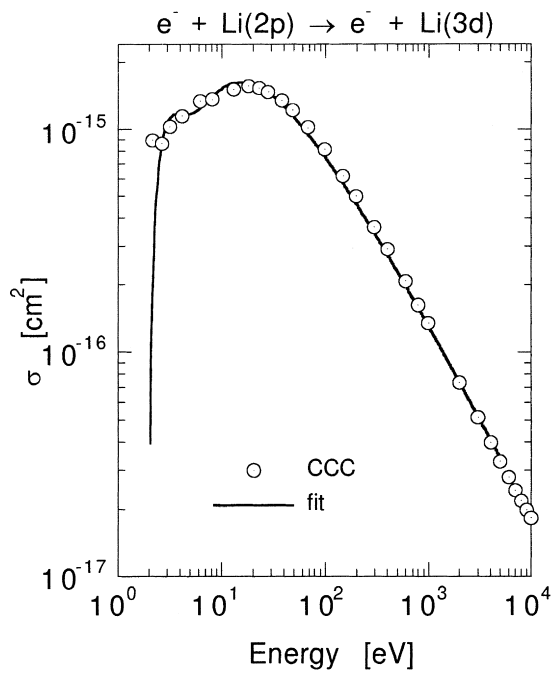
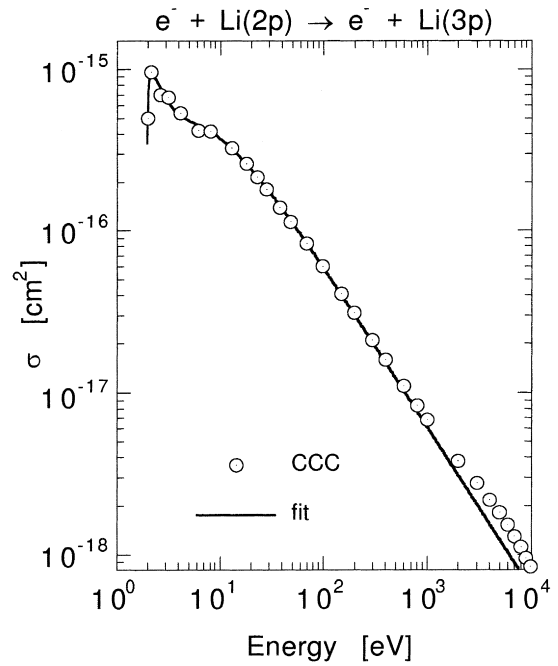
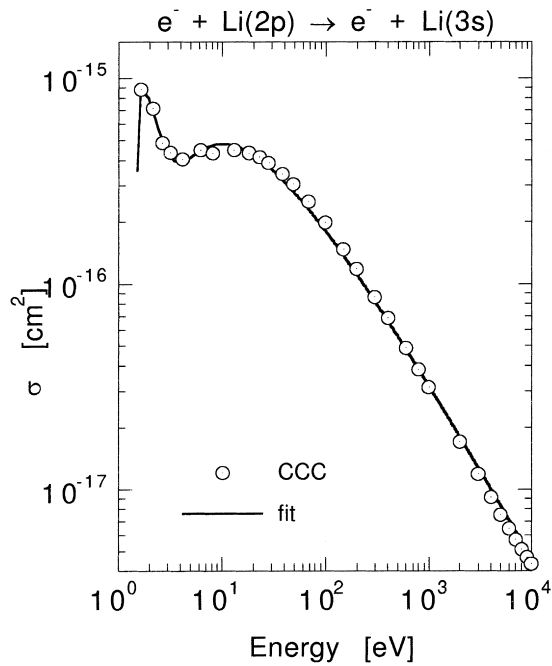
See page 249 for Explanation of Graphs



GRAPHS I 1-36. Electron-Impact Target-Excitation Cross Sections

of  $\text{Li}(nl \rightarrow n'l')$ ;  $n, n' = 2-4$

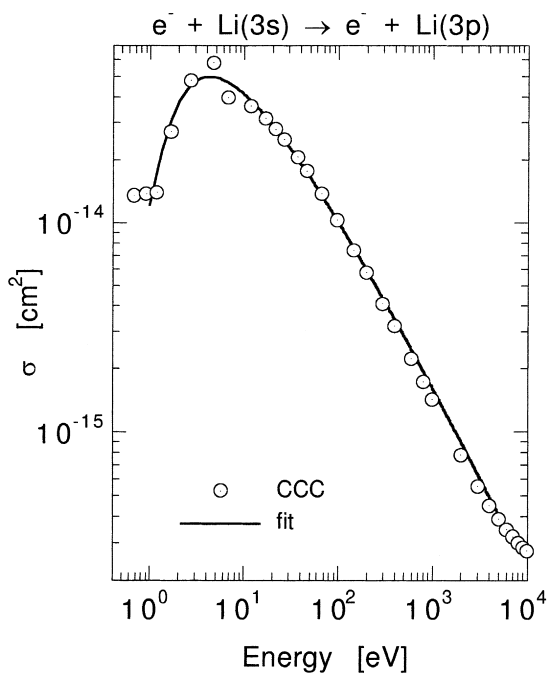
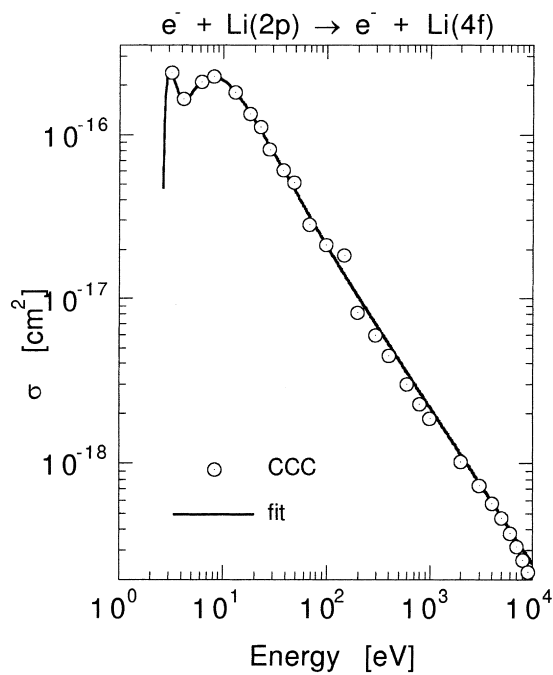
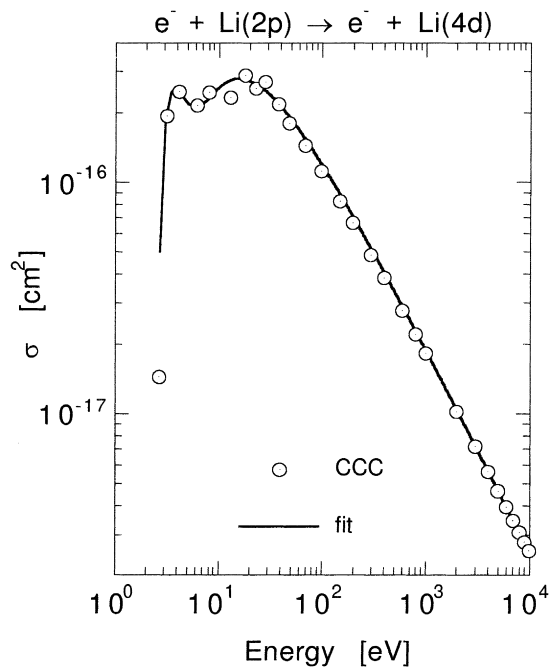
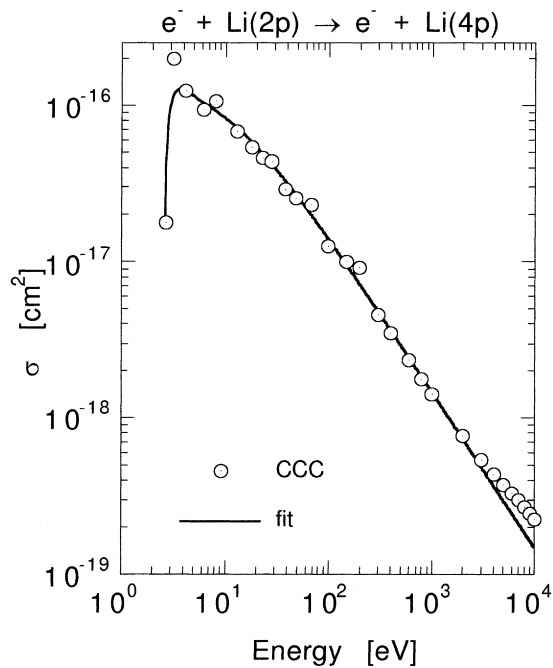
See page 249 for Explanation of Graphs



GRAPHS I 1-36. Electron-Impact Target-Excitation Cross Sections

of  $\text{Li}(nl \rightarrow n'l')$ ;  $n, n' = 2-4$

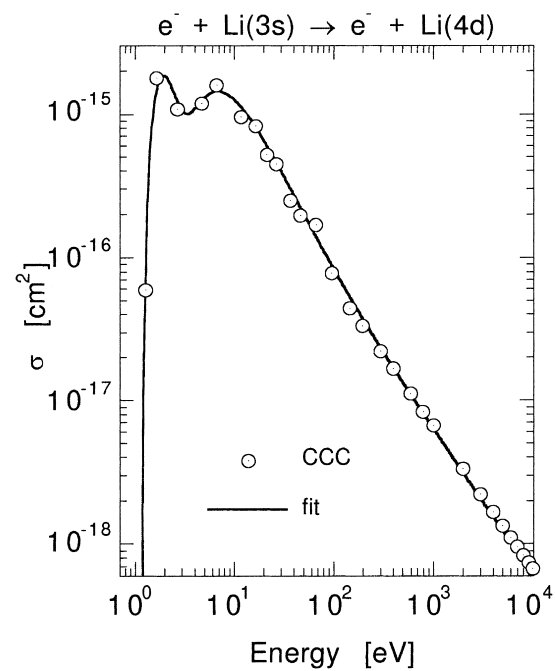
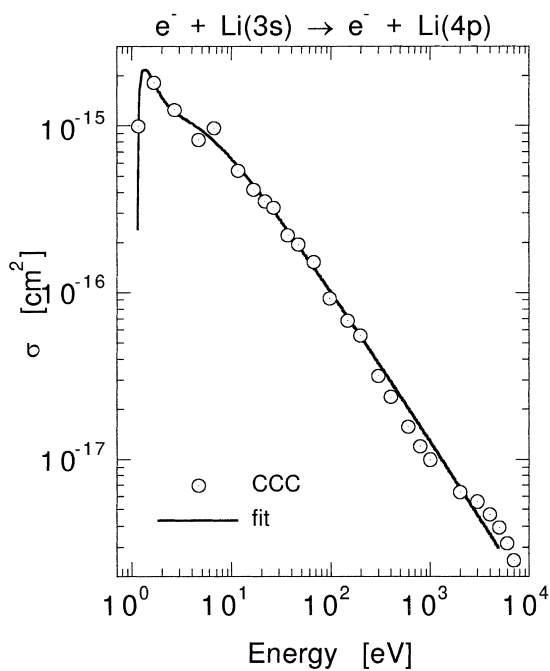
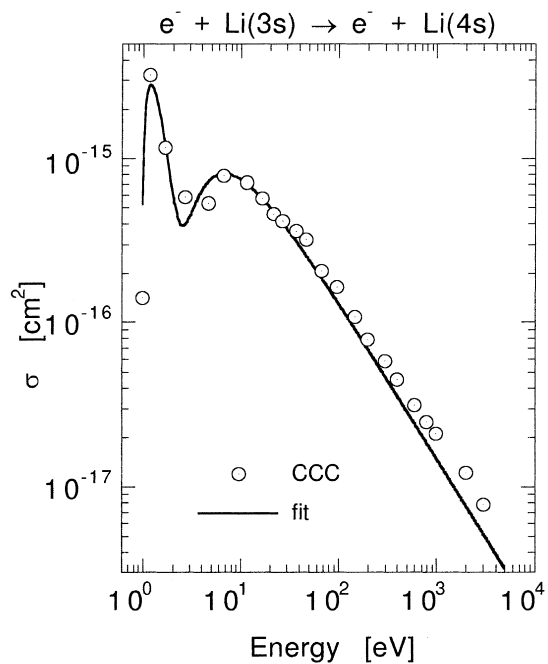
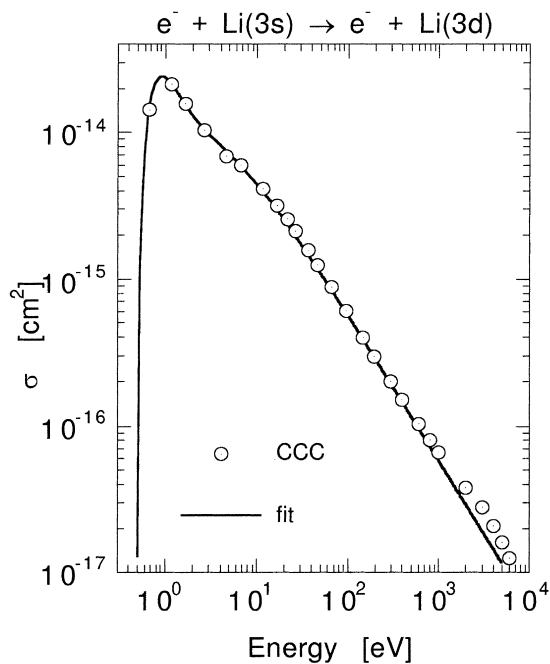
See page 249 for Explanation of Graphs



GRAPHS I 1-36. Electron-Impact Target-Excitation Cross Sections

of  $\text{Li}(nl \rightarrow n'l')$ ;  $n, n' = 2-4$

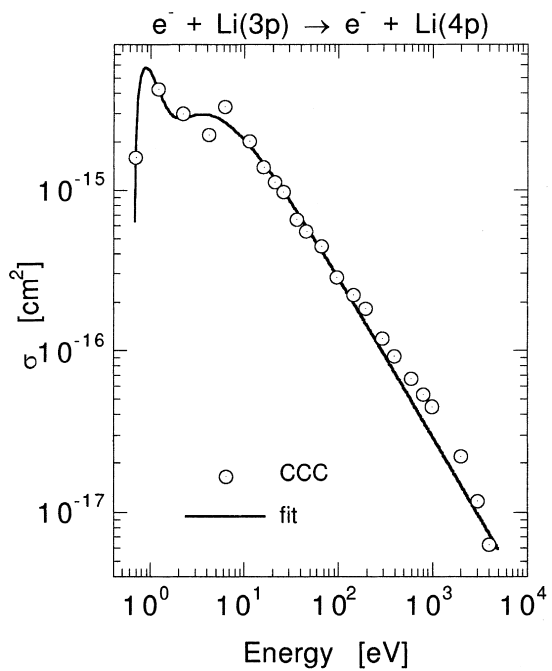
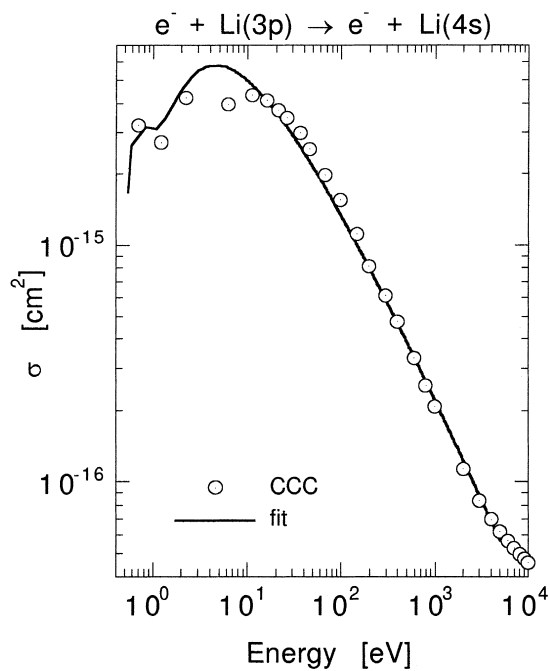
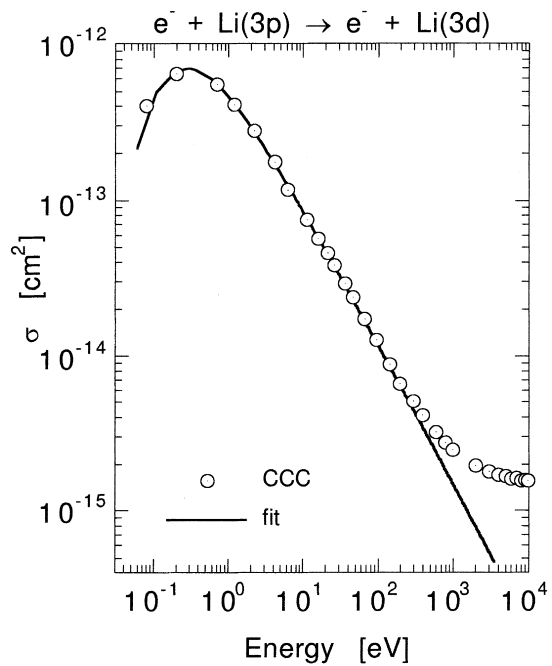
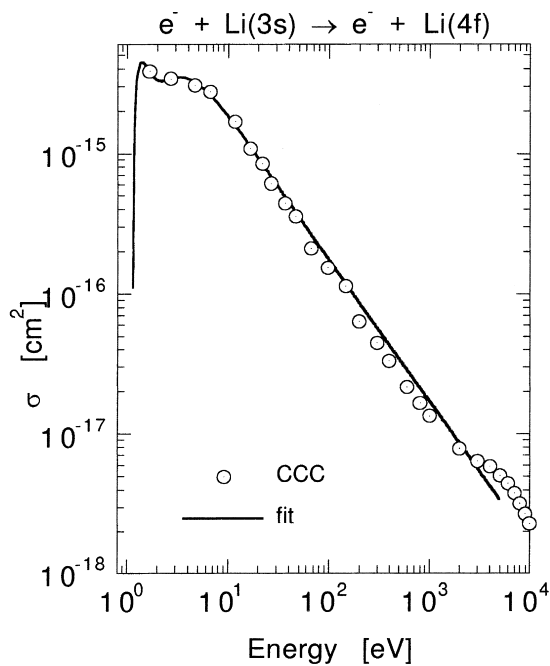
See page 249 for Explanation of Graphs



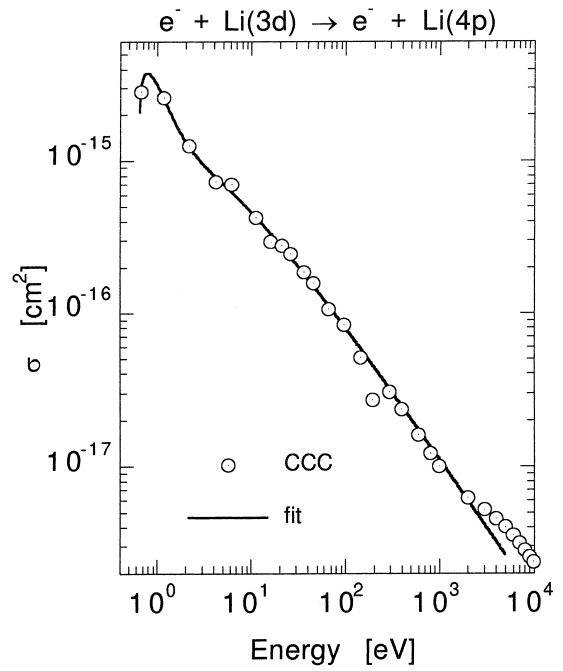
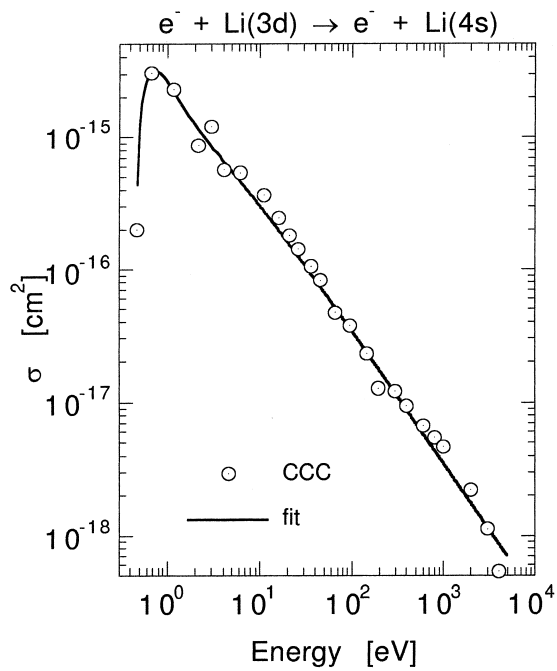
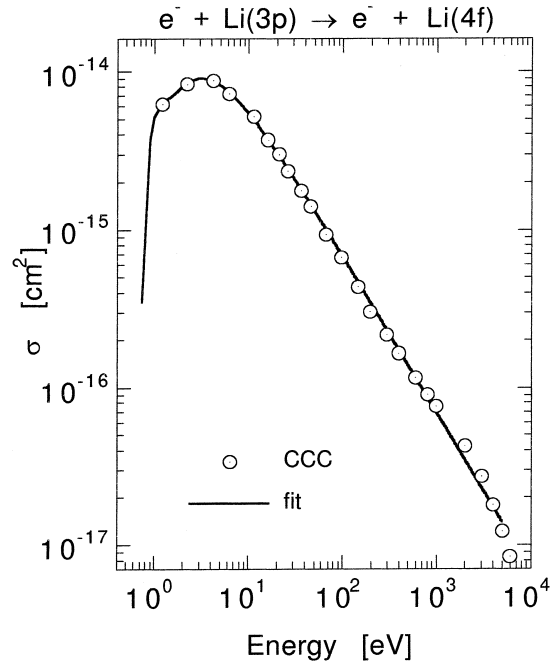
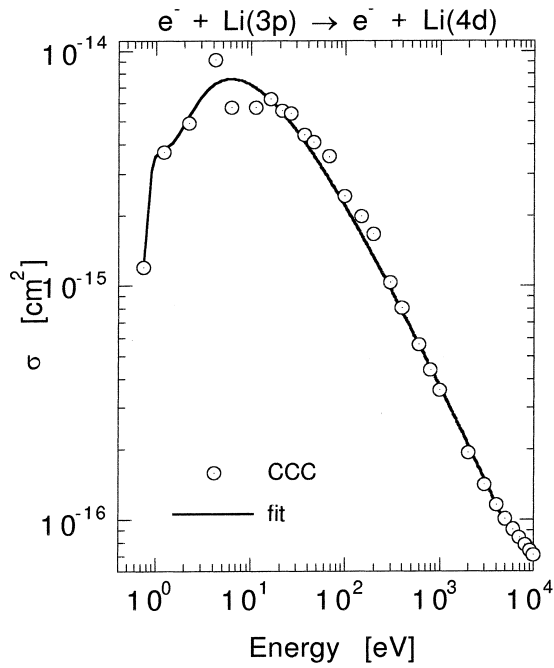
GRAPHS I 1-36. Electron-Impact Target-Excitation Cross Sections

of  $\text{Li}(nl \rightarrow n'l')$ ;  $n, n' = 2-4$

See page 249 for Explanation of Graphs



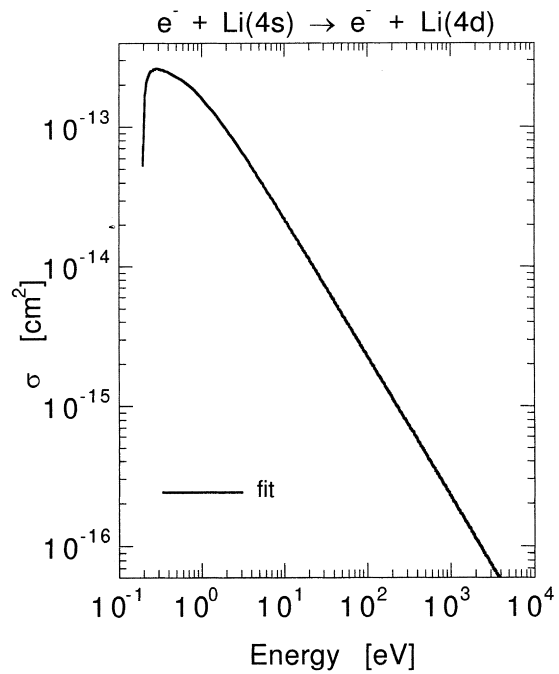
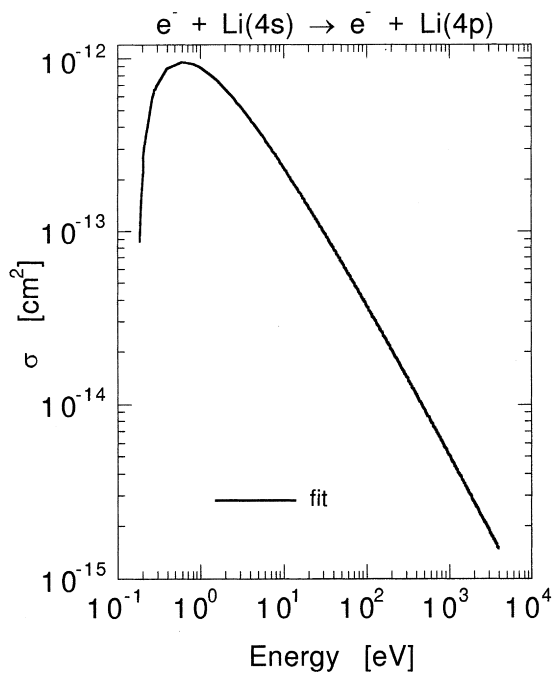
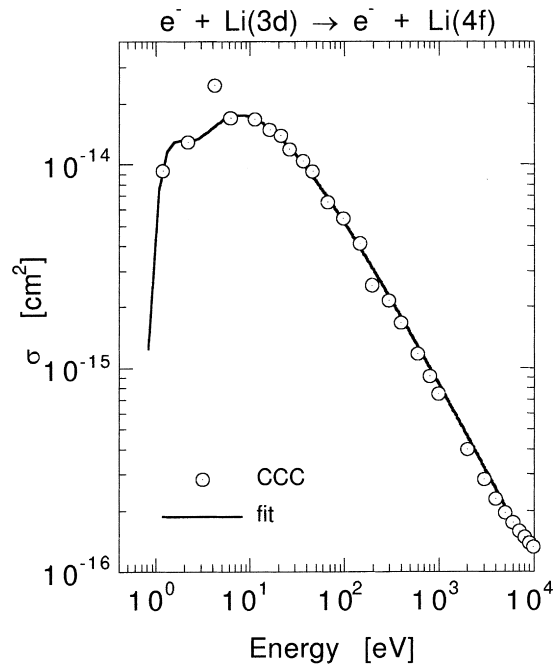
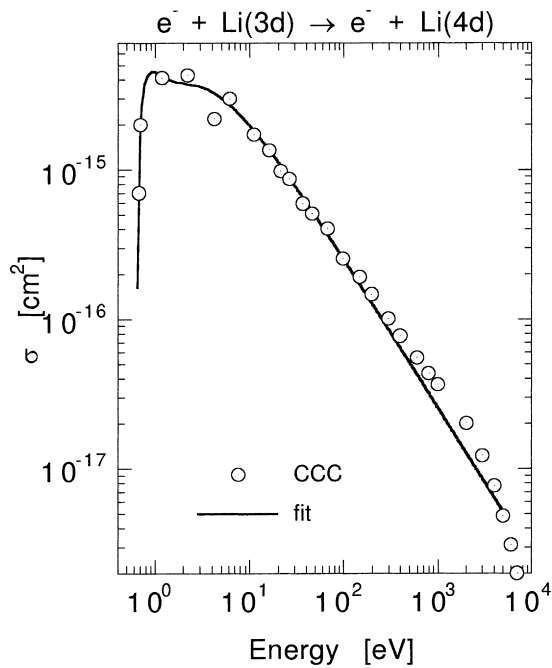
GRAPHS I 1-36. Electron-Impact Target-Excitation Cross Sections  
of  $\text{Li}(nl \rightarrow n'l')$ ;  $n, n' = 2-4$   
See page 249 for Explanation of Graphs



GRAPHS I 1-36. Electron-Impact Target-Excitation Cross Sections

of  $\text{Li}(nl \rightarrow n'l')$ ;  $n, n' = 2-4$

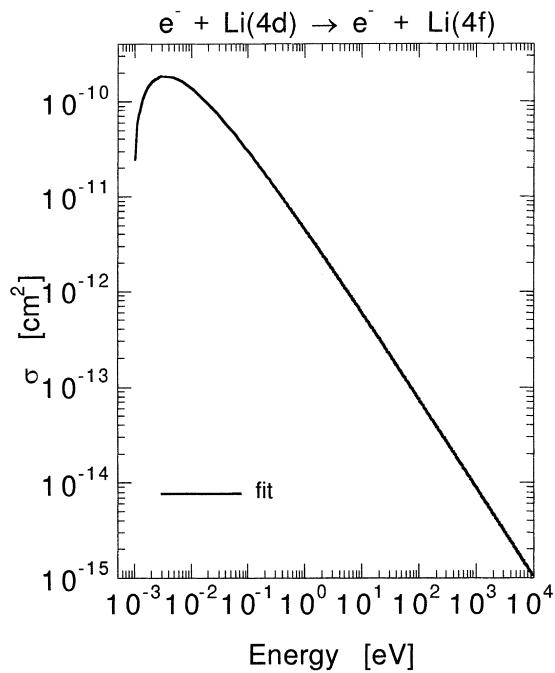
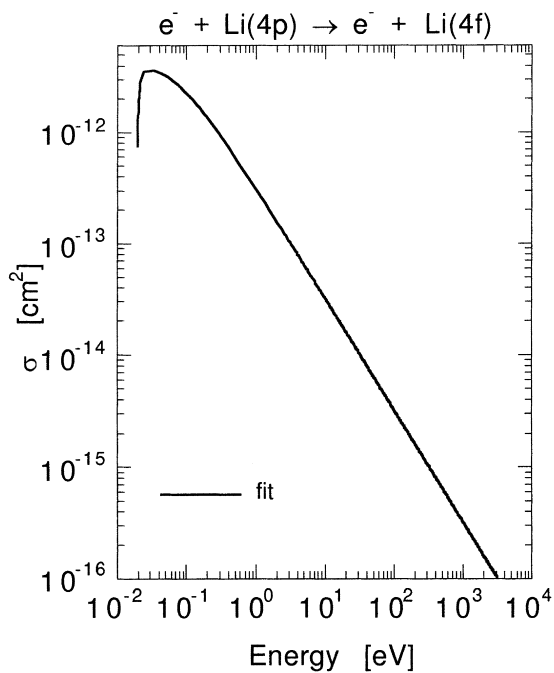
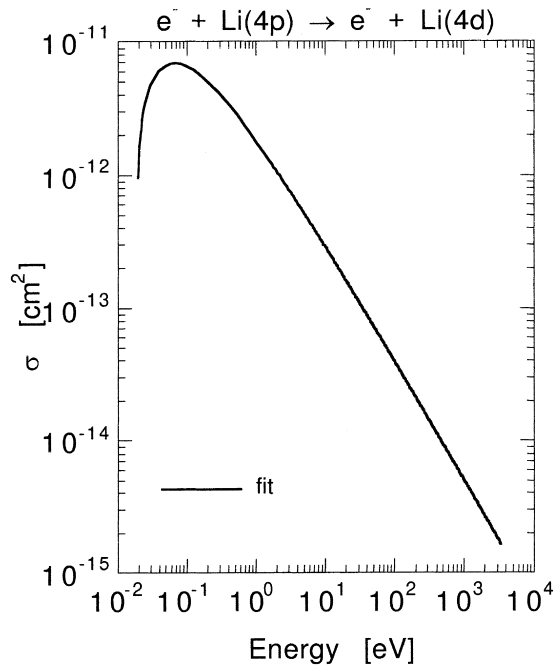
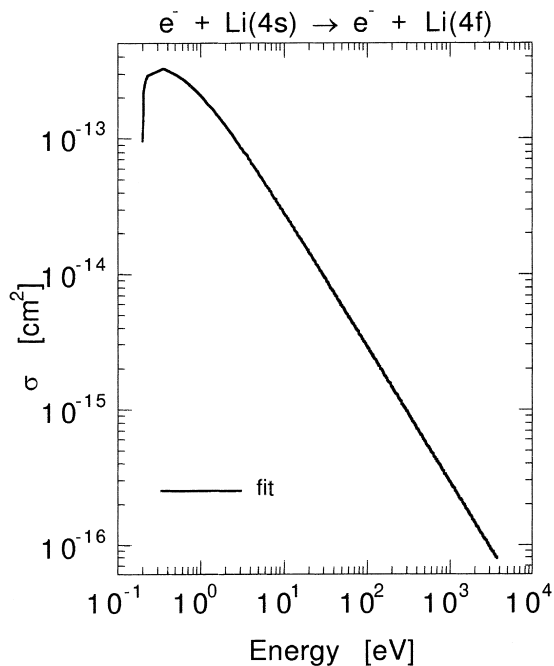
See page 249 for Explanation of Graphs



GRAPHS I 1-36. Electron-Impact Target-Excitation Cross Sections

of  $\text{Li}(nl \rightarrow n'l')$ ;  $n, n' = 2-4$

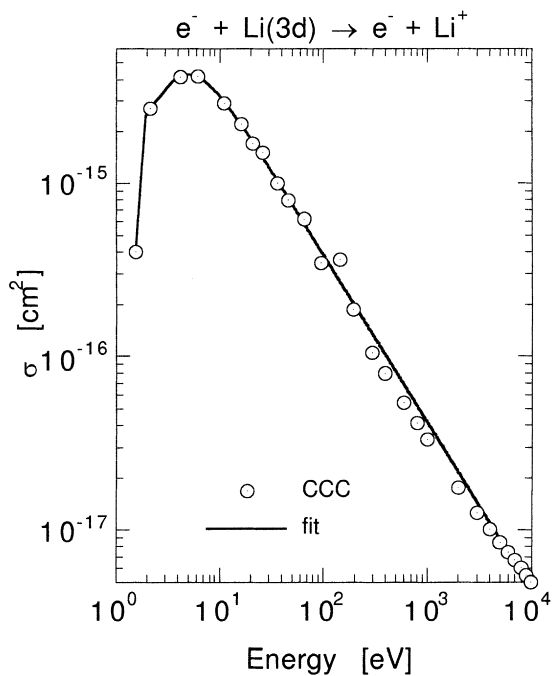
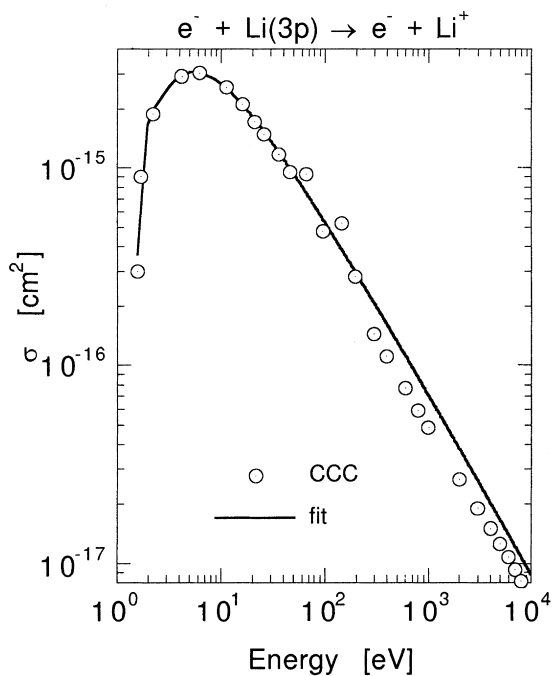
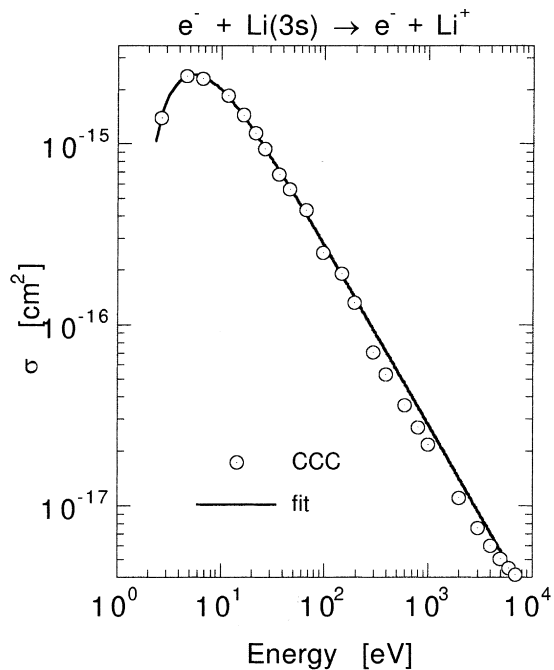
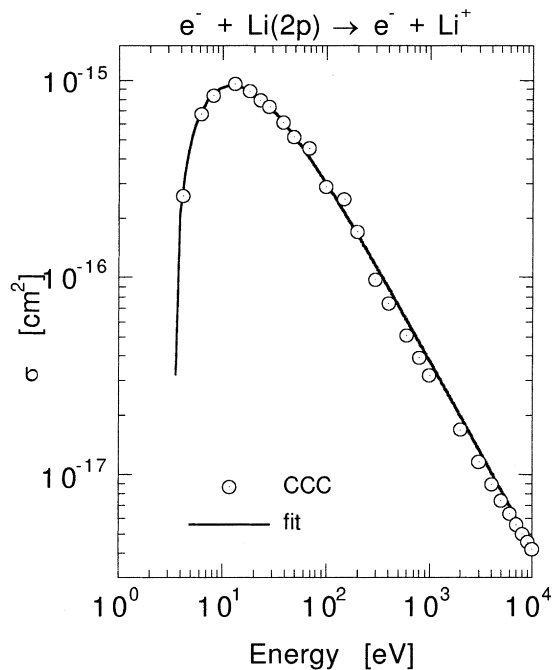
See page 249 for Explanation of Graphs

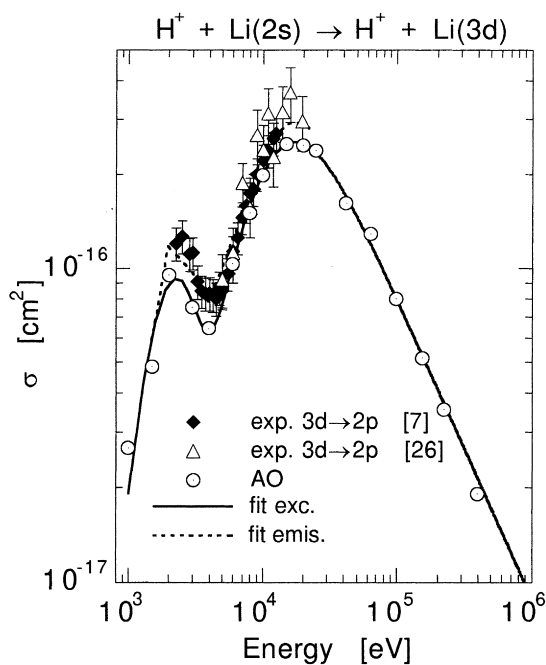
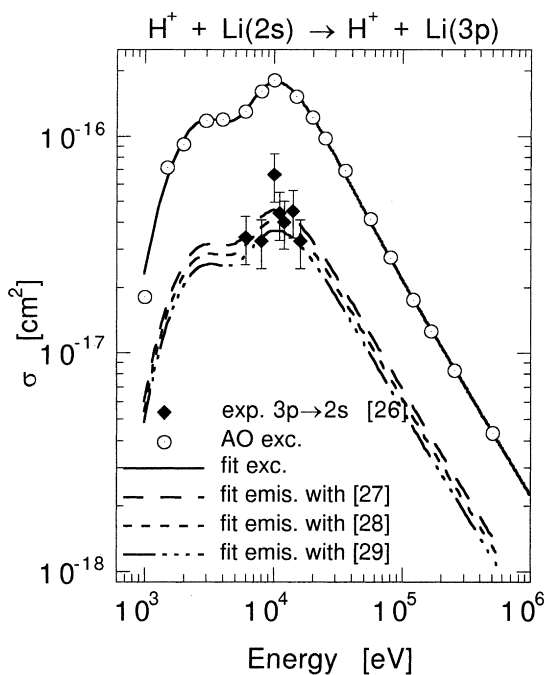
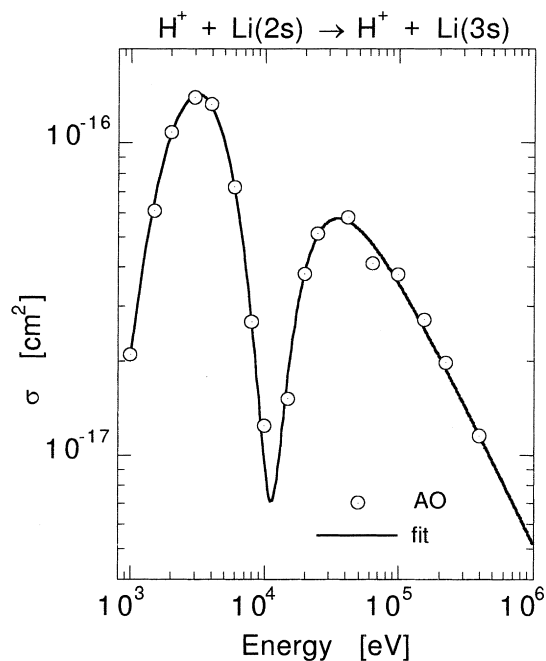
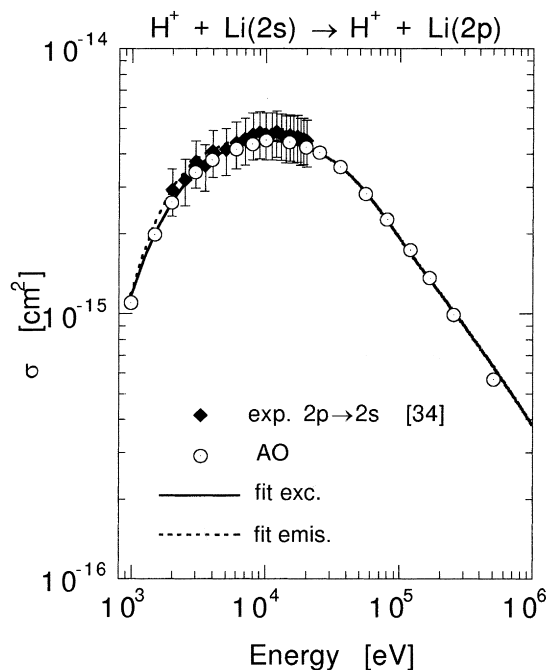


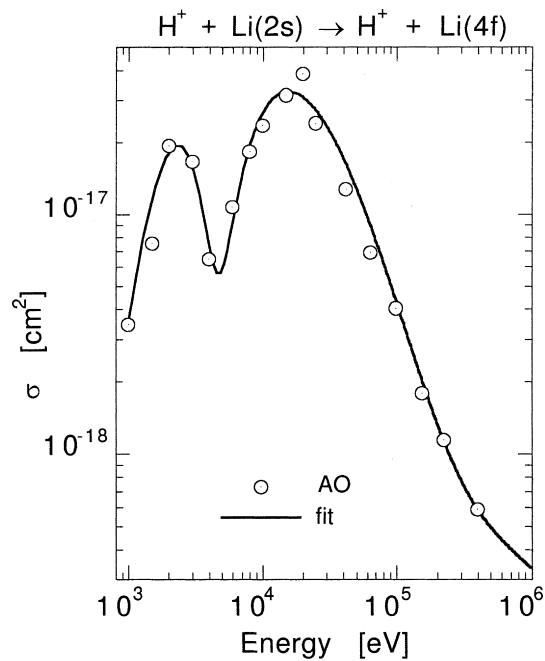
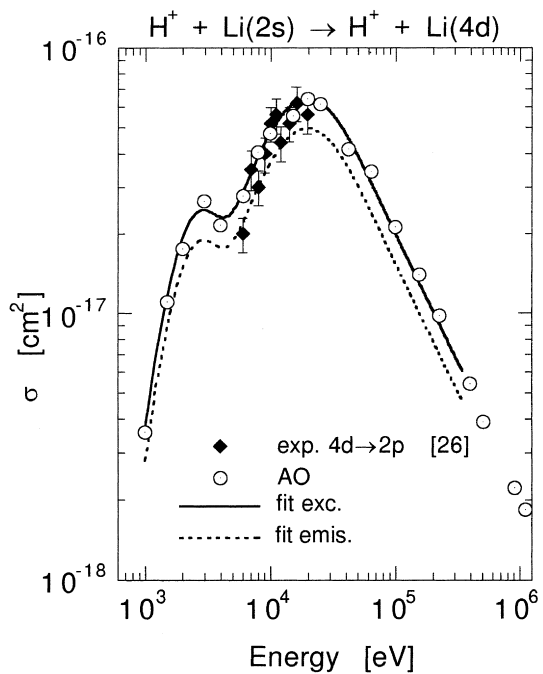
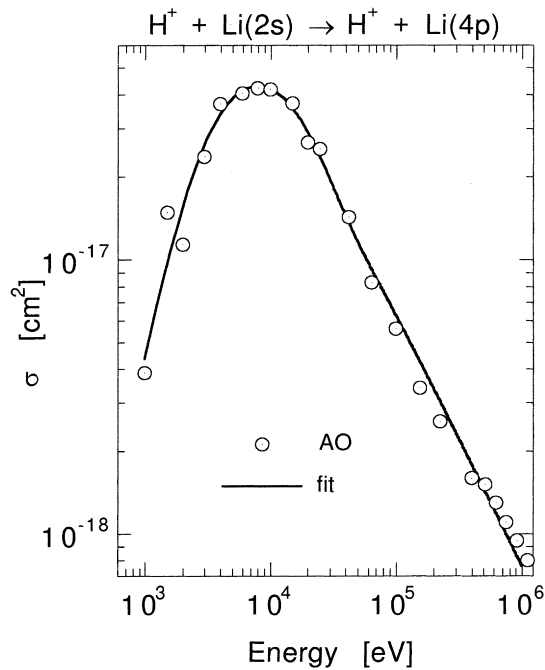
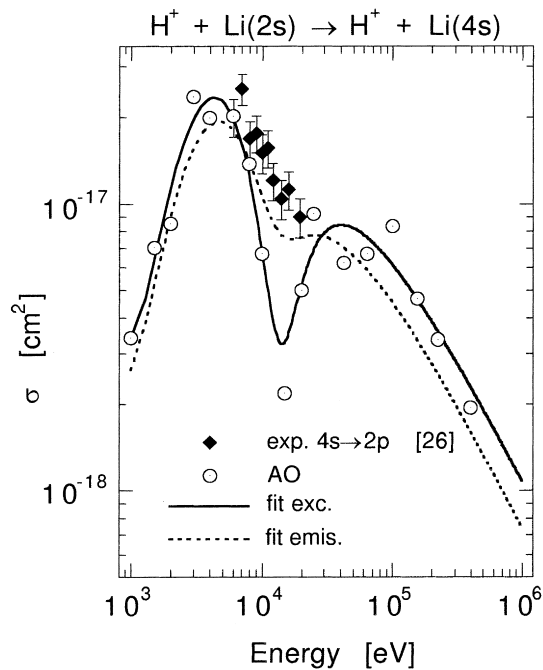
GRAPHS II 1-4. Electron-Impact Target-Ionization Cross Sections

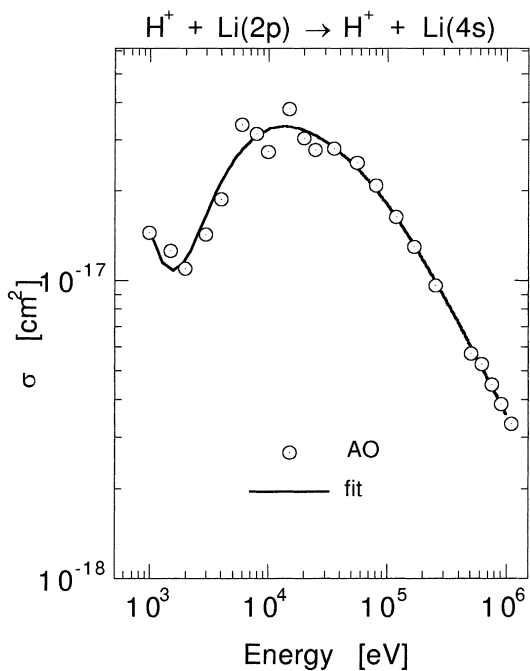
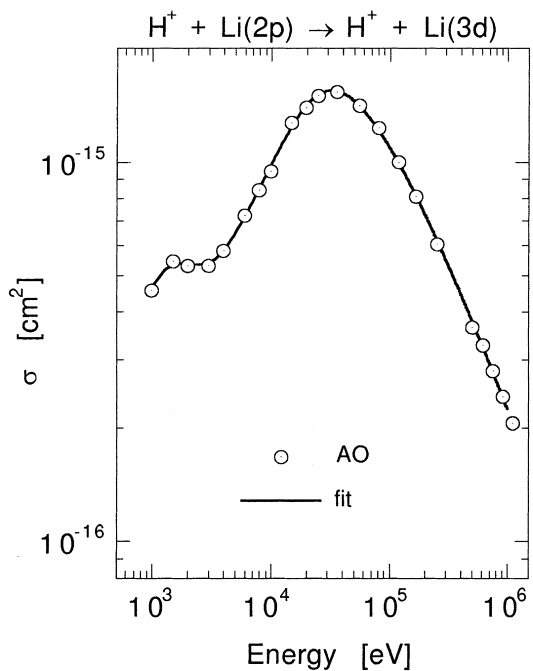
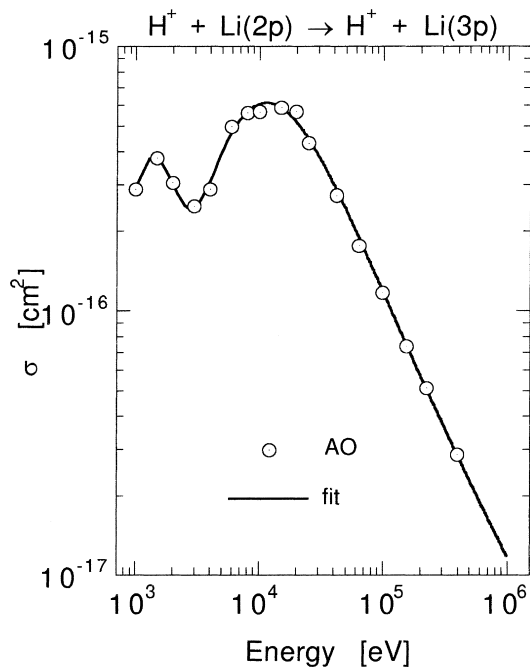
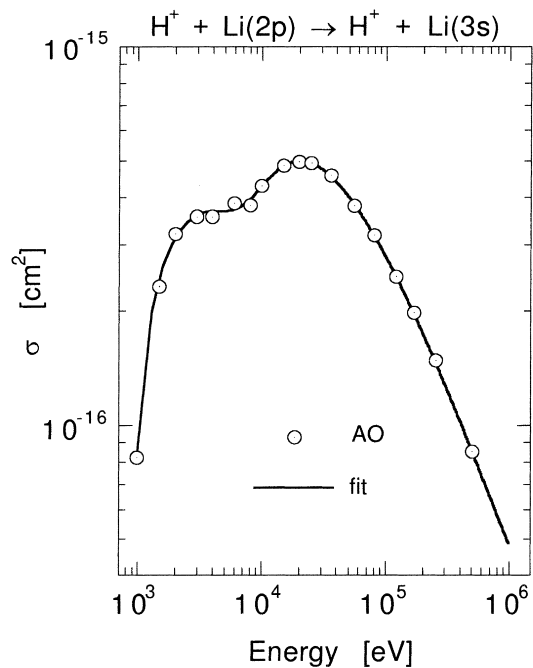
of  $\text{Li}(nl)$ ;  $n = 2, 3$

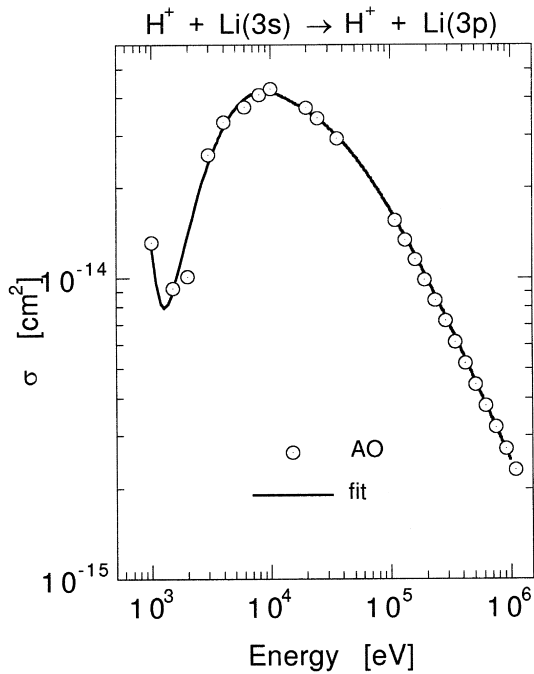
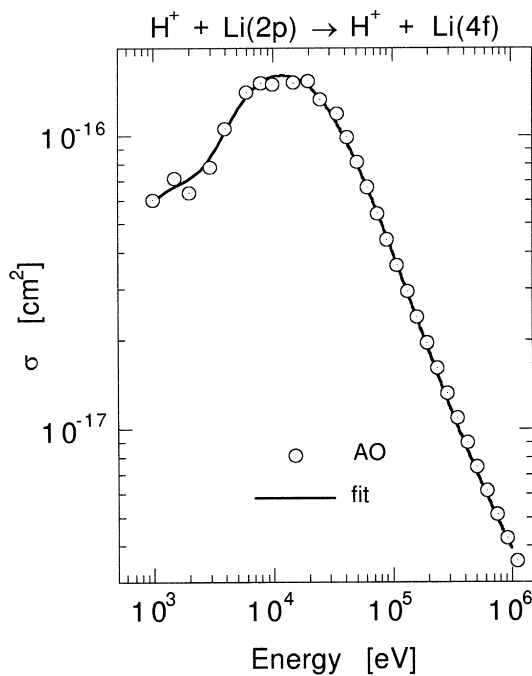
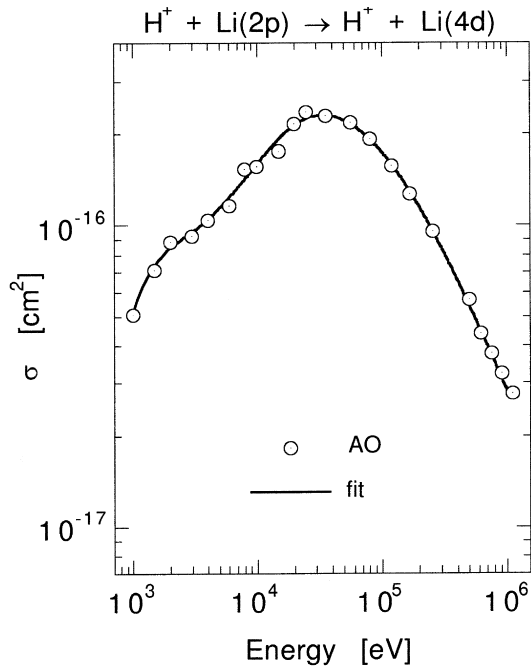
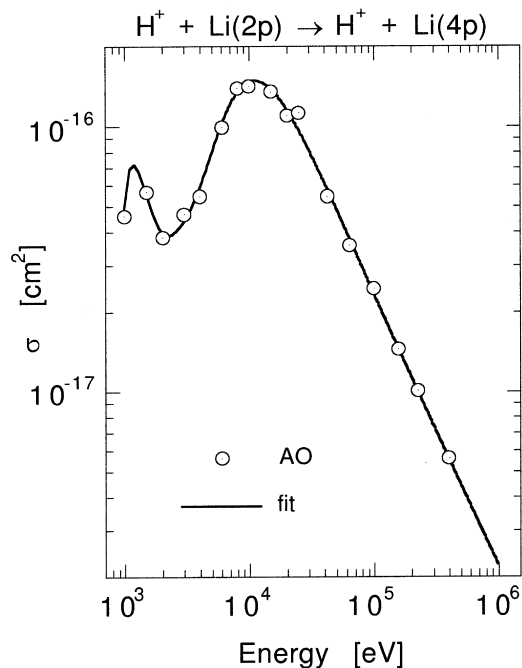
See page 249 for Explanation of Graphs

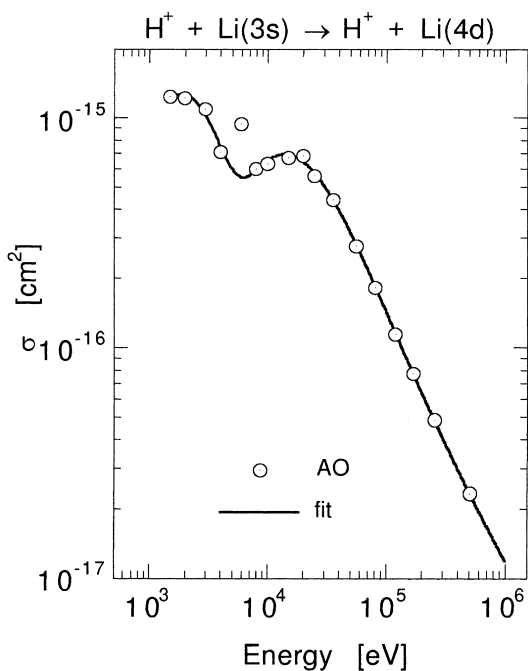
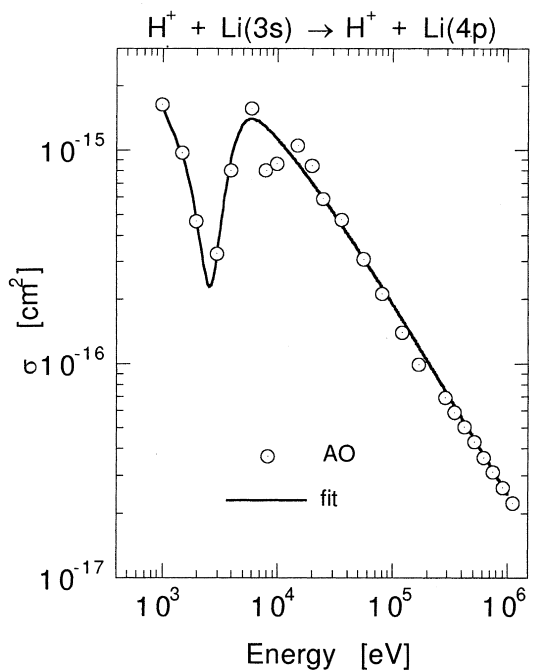
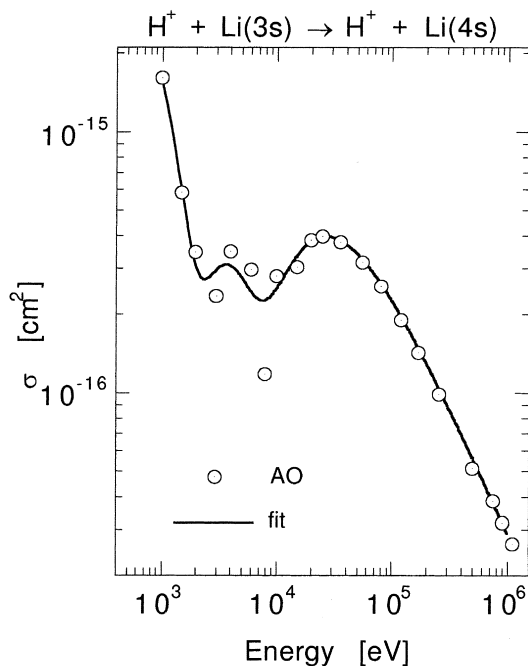
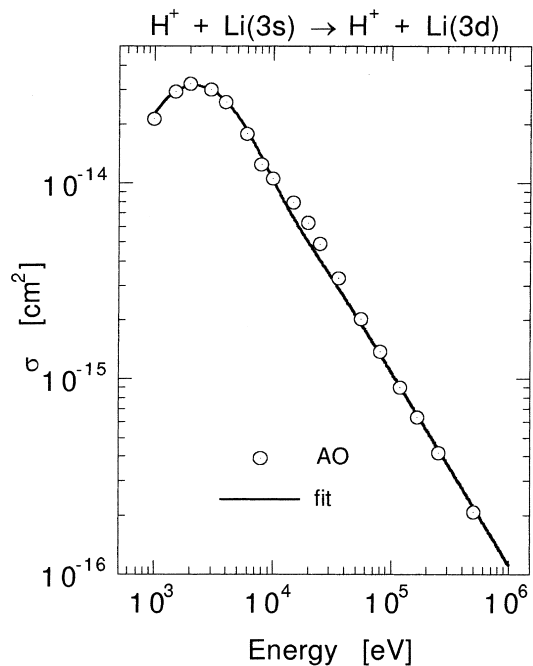




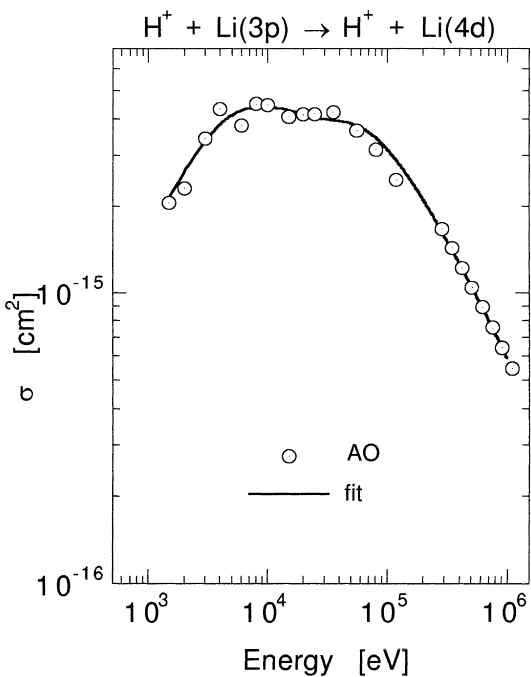
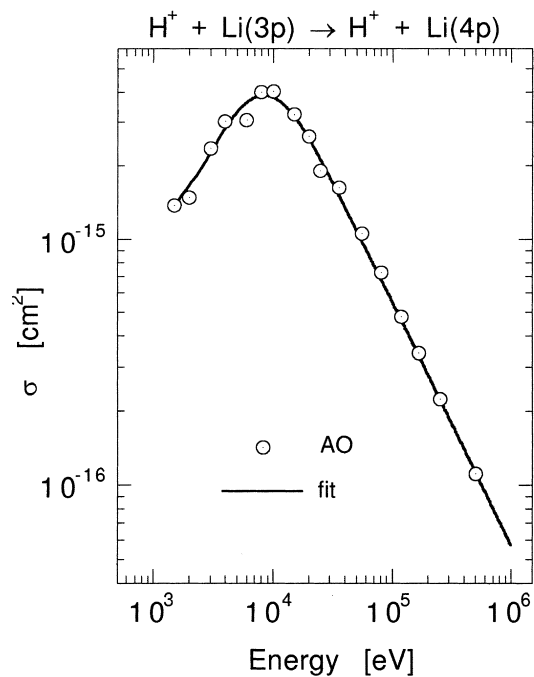
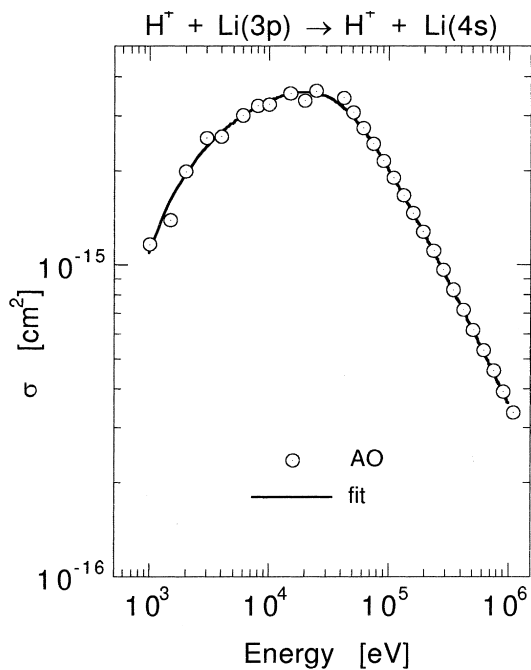
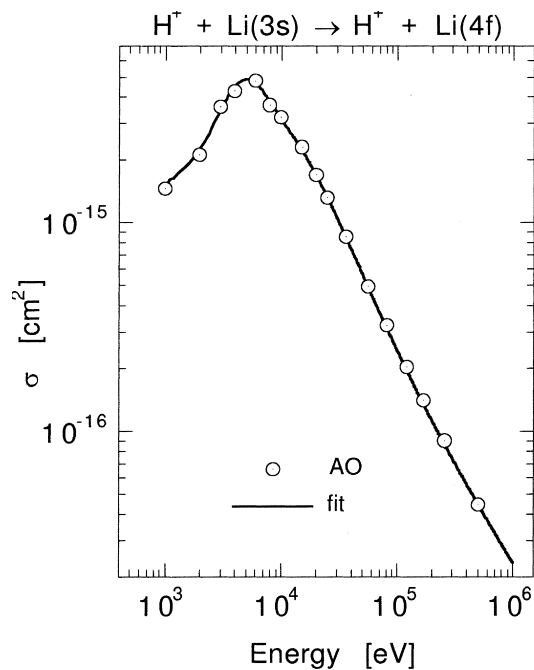








GRAPHS III 1-29. Proton-Impact Target-Excitation Cross Sections of  $\text{Li}(nl \rightarrow n'l')$ ;  
 $n = 2, 3; n' = 2-4$   
 See page 249 for Explanation of Graphs



GRAPHS III 1-29. Proton-Impact Target-Excitation Cross Sections of  $\text{Li}(nl \rightarrow n'l')$ ;  
 $n = 2, 3; n' = 2-4$   
 See page 249 for Explanation of Graphs

